Research Paper

GEOSPHERE

GEOSPHERE; v. 14, no. 4

https://doi.org/10.1130/GES01592.1

15 figures

CORRESPONDENCE: brad.field@gns.cri.nz

CITATION: Field, B.D., Browne, G.H., Fielding, C.R., Florindo, F., Harwood, D.M., Judge, S.A., Krissek, L.A., Panter, K.S., Passchier, S., Pekar, S.F., Sandroni, S., and Talarico, F.M., 2018, A sedimentological record of early Miocene ice advance and retreat, AND-2A drill hole, McMurdo Sound, Antarctica: Geosphere, v. 14, no. 4, https://doi.org/10.1130/GES01592.1.

Science Editor: Raymond M. Russo
Associate Editor: Rhawn Denniston

Received 31 July 2017
Revision received 12 December 2017
Accepted 26 April 2018

A sedimentological record of early Miocene ice advance and retreat, AND-2A drill hole, McMurdo Sound, Antarctica

B.D. Field[1], G.H. Browne[1], C.R. Fielding[2], F. Florindo[3], D.M. Harwood[2], S.A. Judge[4], L.A. Krissek[5], K.S. Panter[6], S. Passchier[7], S.F. Pekar[8], S. Sandroni[9], and F.M. Talarico[9,10]

[1]GNS Science, PO Box 30368, Lower Hutt, New Zealand
[2]Department of Earth and Atmospheric Sciences, 126 Bessey Hall, University of Nebraska-Lincoln, Nebraska 68588- 0340, USA
[3]Istituto Nazionale di Geofisica e Vulcanologia, Via di Vigna Murata 605, 1-00143 Rome, Italy
[4]Department of Geology, College of Wooster, 944 College Mall, Wooster, Ohio 44691, USA
[5]School of Earth Sciences, Ohio State University, 125 South Oval Mall, Columbus, Ohio 43210, USA
[6]Department of Geology, Bowling Green State University, Bowling Green, Ohio 43402, USA
[7]Department of Earth & Environmental Sciences, Montclair State University, 252 Mallory Hall, 1 Normal Avenue, Montclair, New Jersey 07043, USA
[8]School of Earth & Environmental Sciences, Queen's College, 65-30 Kissena Blvd., Flushing, New York 11367, USA
[9]Museo Nazionale dell'Antartide, Università degli Studi di Siena, Via Laterina 8, Siena, Italy
[10]Dipartimento di Scienze Fisiche, della Terra e dell'Ambiente, Università degli Studi di Siena, Via Laterina 8, Siena, Italy

ABSTRACT

The lowest 501 m (~1139–638 m) of the AND-2A core from southern McMurdo Sound is the most detailed and complete record of early Miocene sediments in Antarctica and indicates substantial variability in Antarctic ice sheet activity during early Miocene time. There are two main pulses of diamictite accumulation recorded in the core, and three significant intervals with almost no coarse clasts. Each diamictite package comprises several sequences consistent with ice advance-retreat episodes.

The oldest phase of diamictite deposition, Composite Sequence 1 (CS1), has evidence for grounded ice at the drill site and has been dated around 20.2–20.1 Ma. It likely coincides with cooling associated with isotope event Mi1aa. This is overlain by a diamictite-free, sandstone-dominated interval, CS2 that includes three coarsening-upward deltaic cycles, is inferred to mark substantial warming, and has an inferred age range between 20.1 and 20.05 Ma. Above this is an interval with variable amounts of diamictite (CS3), with indicators of ice grounding, that is inferred to record ice advance relative to CS2, and is overlain by an ~100-m-thick mud-rich interval (CS4) with no sedimentological evidence for direct glacial influence at the drill site (ca. 19.4–18.7 Ma). A third overlying diamictite-rich interval (CS5) overlies an unconformity spanning 18.7–17.8 Ma (coinciding with isotope event Mi1b), and records a return to more ice-influenced conditions at the drill site in late early Miocene time. The overall picture for the early Miocene (spanning the period 20.2–17.35 Ma) is one of ice advance alternating with periods of ice retreat and hence significant global climate fluctuations after the permanent establishment of the Antarctic ice sheet at the Eocene/Oligocene boundary, and preceding the relative warmth of the middle Miocene climatic optimum (ca. 17.5–14.5 Ma).

Sedimentary cyclicity in CS1 and CS2 is consistent with ~21 k.y. precession but in CS3 the frequency is closer to 100 k.y. (consistent with eccentricity), with a possible change to 20 k.y. precession in CS4. CS5 cyclicity is consistent with obliquity forcing. Provenance data are consistent with local Transantarctic Mountains glacial activity under precessional control in CS1 and more southerly ice-cap build up under 100 k.y. eccentricity and obliquity control during CS3 and CS5, respectively.

INTRODUCTION

The Antarctic Geological Drilling Program (ANDRILL) aimed to provide proximal records of Antarctic Cenozoic ice sheet advance and retreat previously inferred from far-field deep sea stable isotope records (e.g., Shackleton and Kennett 1975; Zachos et al., 2001) and passive margin eustatic sea-level reconstructions (e.g., Kominz et al., 2008), to better constrain climate models and predictions of the effects of future climate change. An earlier drill hole, ANDRILL-1B, was drilled near to McMurdo Station/Scott Base and provided a detailed record of part of the late Miocene and of Pliocene relative warm events for Antarctica (McKay et al., 2009; Naish et al., 2009). AND-2A was drilled in southern McMurdo Sound in October-November 2007 (Harwood et al., 2008; Fig. 1). AND-2A was located at 77° 45.488′S 165° 16.613′E and drilled from an 8.5-m-thick floating sea-ice platform. It recovered a 1138.54 m long drill core spanning early Miocene to Pliocene time, though with substantial parts of the early, middle and late Miocene and Plio-Pleistocene record absent due to the presence of erosional unconformities. The facies have been described and interpreted by Passchier et al. (2011), and the stratigraphy and sequences have been described by Fielding et al. (2008, 2011; Figs. 2 and 3). These papers set out the broad stratal relationships observed from core-based sedimentological studies. Levy et al. (2016) reviewed the evidence for glacial advance and retreat and found diamictites were likely deposited by ice rafting during cold periods (see also the companion modeling paper, Gasson et al., 2016). The present study describes in greater detail relationships observed in early Miocene sediments in the lowest 501 m of the drill hole, and a major unconformity within the early Miocene at 778 m (all depths are cited in meters below the sea floor).

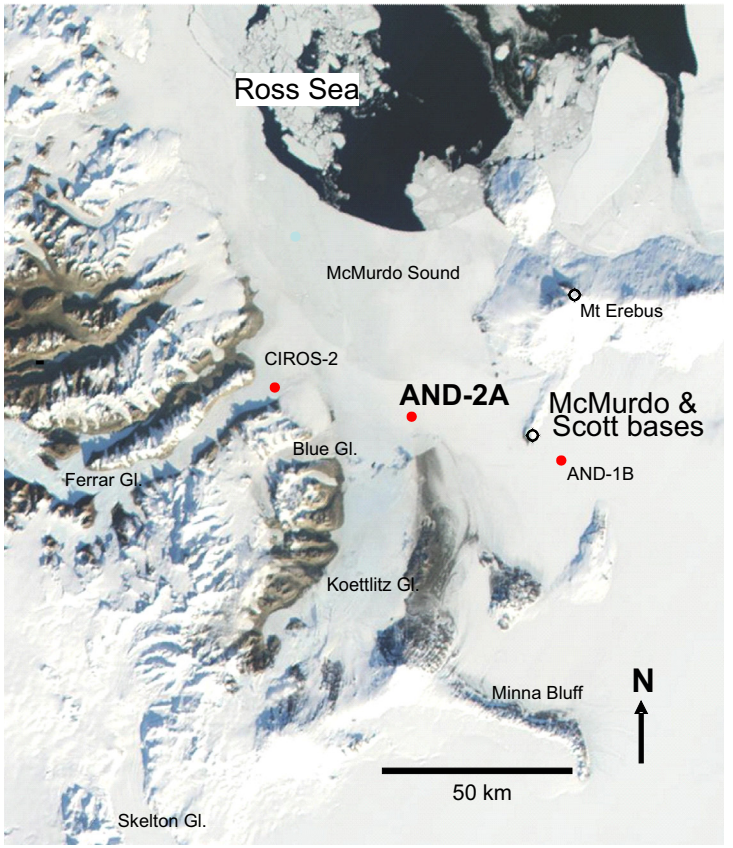

Figure 1. Location of the AND-2A drill hole, southern McMurdo Sound, Antarctica. Gl—glacier.

Prior to the drilling of AND-2A the only other thick, proximal sedimentary record of events during the early Miocene in the western Ross Sea region was drill hole CRP-1 (Cape Roberts Project site) (Barrett, 1998). This study found evidence for ice advance and retreat in sediments dated 22–17 Ma, as well as evidence of contemporaneous volcanism. In Prydz Bay, East Antarctica, Hannah (2006) inferred early Miocene variations in ice extent based on palynomorphs, noting a change from maximum ice to minimum ice extent between 22 and 19 Ma followed by a return to a cold climate in the period 19–17 Ma. Lear et al. (2004) presented benthic foraminifer Mg/Ca ratios at Ocean Drilling Project (ODP) Site 1218 (equatorial Pacific) which suggest ~2 °C of deep ocean warming between ca. 20.5 and 19.5 Ma. Stable oxygen isotope data from the Kerguelen Plateau (ODP Southern Ocean Site 747) indicate overall warming between ca. 20 Ma and 19 Ma, punctuated by 2–3 episodes of cooling, with substantial cooling around 18 Ma (Shevenell and Kennett, 2007; after Billups et al., 2002). Both palynomorphs and far-field oxygen isotope records thus indicate significant variations in global paleoclimate during the early Miocene. Indeed, Pekar and DeConto (2006) inferred from far-field oxygen isotope records the loss of both the Greenland ice sheet and the West Antarctic Ice Sheet (WAIS), as well as part of the East Antarctic Ice Sheet (EAIS) occurred between 22 and 18 Ma. AND-2A thus provides a unique record of the effects of climate change on the margin of Antarctica during early Miocene time and brings insight to early Miocene climate change relative to younger proximal records of middle Miocene to Pleistocene ice sheet dynamics (e.g., McKay et al., 2009; Naish et al., 2009; Pollard and DeConto, 2009; Sandroni and Talarico, 2011; Hauptvogel and Passchier, 2012). The early Miocene is shown to be a period of substantial and frequent variability in ice extent, and adds to growing evidence that at geologic time scales the extent of the Antarctic ice sheet is characterized by dynamic change rather than stability.

CORE CHARACTERIZATION OF AND-2A

The core was scanned and logged for fractures and petrophysical properties, then slabbed to produce an archival half and a working half. The working half of the core was sedimentologically logged at McMurdo Station within days of recovery to ensure minimal handling disturbance and alteration. The core was logged by the team at cm-scale and this same half was later sampled for paleomagnetism, paleontology, geochemistry, petrology and petrophysics. Lithologic features were used to distinguish a variety of lithofacies and combinations of these were used to distinguish fourteen, larger-scale lithostratigraphic units (LSUs) over the 1138 m of recovered core (Fielding et al., 2008; Passchier et al., 2011). Smear slides were examined during initial core logging at McMurdo at generally one-meter intervals over the entire core, providing initial estimates of variation in grain size, biogenic material, and volcanic glass (Fielding et al., 2008; Panter et al., 2008).

Fielding et al. (2011) divided the entire cored succession into 74 high-frequency (fourth or fifth order) glacimarine sequences recording repeated advances and retreats of glaciers into and out of the Victoria Land Basin; these can be resolved into thirteen longer-term, composite sequences (third order; CS1-13), each characterized by one of six sedimentary motifs that comprise distinct assemblages of facies (Fielding et al., 2011; Passchier et al., 2011). These motifs build on the three recognized by McKay et al. (2009) in AND-1B and largely represent facies deposited in more ice-distal settings in AND-2A compared to those represented in AND-1B (table 1 of McKay et al. [2009]). The early Miocene composite sequences (CS1–CS5) are comparable with lithostratigraphic units (LSU) 14–10 of Fielding et al. (2008) and are the focus of this paper.

An ice-proximity record was established, ranging from ice-loading features such as unstratified diamictite with boxwork fractures, jigsaw-fit breccias, and rotational and other shear structures indicating pressure from overlying, grounded ice (of glaciers or icebergs; Fielding et al., 2008, 2011; Passchier et al.,

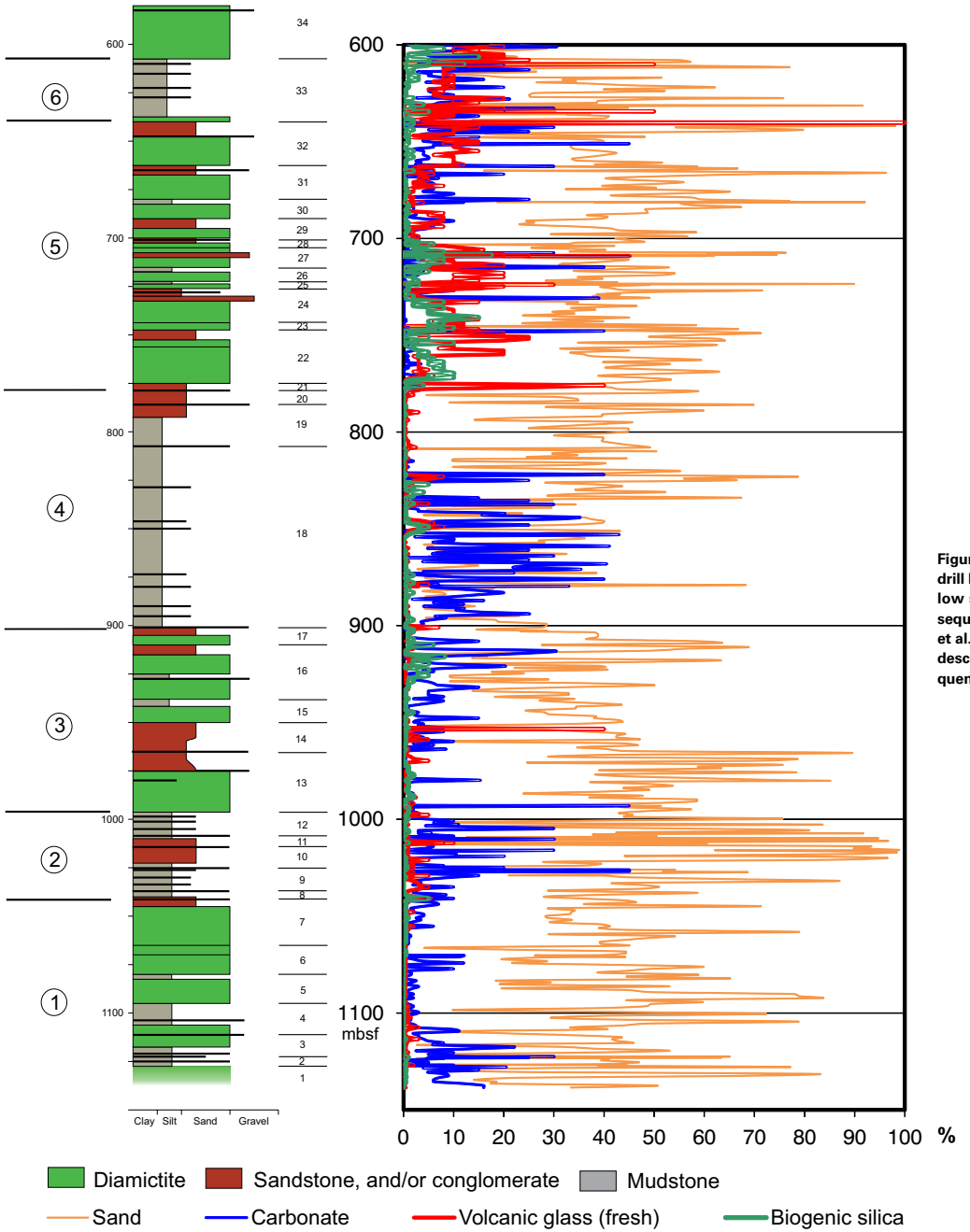

Figure 2. Summary log, for the AND-2A drill hole, of depths greater than 600 m below seafloor [mbsf], showing composite sequence subdivisions used (after Fielding et al., 2011). The five composite sequences described in this paper are labeled 1–5. Sequence 6 is shown to add context.

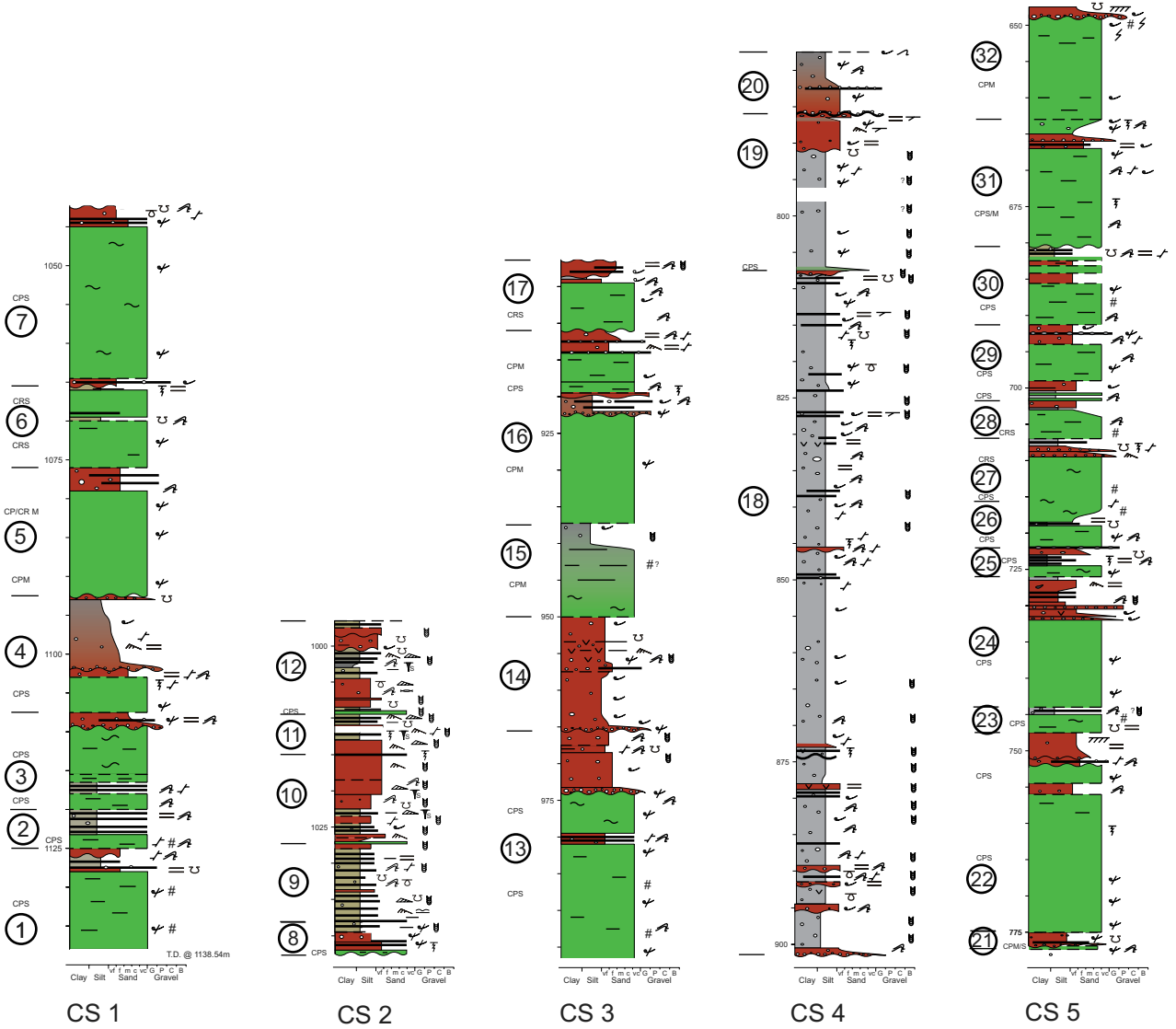

Figure 3. (A) Early Miocene composite sequences (CS1 to CS5) between 775 and 1145 m and their component sequences (after Fielding et al., 2011). Note the contrasts between CSs 2 and 4 with CSs 1, 3, and 5. See Figure 2 for a key to colors in the lithologic column and (B) for graphics symbols. Numbered intervals refer to the cycles recognized by Fielding et al. (2011). Abbreviations: vf—very fine; f—fine; m—medium; c—coarse; vc—very coarse; G—granule; P—pebble; C–cobble; B—boulder. T.D.—total depth; CPS—clast-poor, sandy; CRS—clast-rich, sandy; CP/CR M—clast-poor/clast-rich, muddy; CPM—clast-poor, muddy; CPS/M—clast-poor, sandy/muddy; CPM/S—clast-poor, muddy/sandy.

2011), through to diatomite with no lonestones indicating ice-free conditions at the drill site. Intervals of sandstone and mudstone with <1% lonestones indicate intermediate depositional settings with ice present near to the drill site (units with 1% or more of granule or coarser clasts were classified as diamictite after Naish et al., 2006). Parallel studies have included detailed paleontology, petrology, geochemistry and radiometric dating, and grain size analyses (e.g., Passchier et al., 2013), and chemical index of alteration data (CIA), along with TEX_{86} paleotemperature data, have helped refine interpretations of ice proximity (Levy et al., 2016).

High-resolution digital images of the core were later studied in more detail using Visualizer (Josh Reed, personal commun., 2010) and have been used to provide further detailed analysis as part of this study.

AGE MODEL

Our age model is based on Acton et al. (2008) and Di Vincenzo et al. (2010) which incorporates ^{40}Ar-^{39}Ar ages from volcanic clasts and tephra layers, $^{87}Sr/^{86}Sr$ dating of macrofossil shells, paleontology (diatoms in particular), and magnetostratigraphy using the geological polarity time scale of Gradstein et al. (2004) and is, in general, internally consistent. A later revision to the interpretation gives diatom last occurrence age data more weight (SMS Science Team, 2010) with an inferred unconformity at the base of CS5, rather than its top, revising the age of the base of the CS from ca. 18.5 to ca. 17.5 Ma. We use the SMS Science Team (2010) age model (Fig. 4), as also followed by Fielding et al. (2011), and largely matches Levy et al. (2016) though the position of the major unconformity at the base of CS5 is tentatively placed slightly lower (778.34 m rather than 774.94 m—see description and discussion of CS5 below).

PALEOGEOGRAPHIC CONTEXT

The Ross Sea area forms part of the Cenozoic Victoria Land Basin of the West Antarctic Rift, a north-south–trending rift which began to form in Eocene–early Oligocene time (Henrys et al., 2007; Fielding et al., 2008). The main rifting phase was during the early Oligocene to early Miocene (Fielding et al., 2008). The paleogeography of the Ross Sea region during the early Miocene is not well constrained, although improved understanding has come from recognition that Mount Morning appears to have been an active volcano during much of this time (Panter et al., 2008; Di Roberto et al., 2012; Nyland et al., 2013) and that the sedimentary record contains a decipherable history of the interaction of local Transantarctic Mountains (TAM) glaciers and those farther to the south (Talarico and Sandroni, 2011).

Talarico and Sandroni (2011) distinguished three main source areas of extraformational clasts feeding into the study area and interpreted the lithologic provenance signals from them:

- local sources coming from the Royal Society Range to the southwest-west of the drill site (Koettlitz-Blue glaciers region, KB);
- southern sources (Skelton-Mulock glaciers region, SM); and
- far-south sources from the Carlyon Glacier and Darwin-Byrd glaciers area (CB).

Recognition of varying provenance signals over time enabled Talarico and Sandroni to erect several models of glacial transport (their figure 3). When debris derived solely from the regions of the southern glaciers was present along with evidence for ice-sheet grounding at the drill site, this argues for expansion of the EAIS. Under such conditions, the polar ice sheet could have blocked the supply of clasts from the Royal Society Range (KB). When the EAIS was of lesser extent, during more temperate to sub-polar conditions, the local glaciers of the Royal Society Range close to the drill site could have provided significant material. We note, however, that boxwork fabrics and other evidence of ice grounding could occur from either a grounded ice sheet or from grounding of large icebergs during ice-sheet breakup.

Where there is no evidence for ice-sheet grounding at the drill site, then ice-rafted clasts indicate iceberg rafting consistent with calving during breakup (warming). Under these conditions, local TAM glacier grounding lines likely retreated inland of the coastline and would have been unable to contribute ice-rafted local clasts. However, where clasts from both southern and local glaciers are missing, or very sparse, and there is no evidence for ice-grounding, then conditions were likely cold enough that clasts were locked up in the provenance area, but not so cold that grounded ice of the EAIS reached the drill site (Levy et al., 2016).

The sedimentary record of volcanism indicates the timing of crustal-scale uplift events, and hence provides clues to likely changes in the potential provenance of sedimentary clasts. Nyland et al. (2013) noted that higher glass volumes in sediments correlate with ice minimum conditions between 300 and 800 m in AND-2A (ca. 16–19 Ma) and that magmas erupted during ice-minimum conditions are slightly more acidic than those erupted during ice-maxima periods. This suggests that ice thickness (>500 m) and loading were sufficient to affect the upper crustal magma system. An increased abundance of scoria clasts is associated with elevated glass percentages both below and above 800 m in the core (Panter et al., 2008).

The angularity of the glass fragments indicates most glass is primary ashfall material or rainout from sea ice melt (Nyland et al., 2013) rather than reworked from older sediments. The only known source of early Miocene volcanics in the area is Mount Morning, ~100 km to the south of the drill site (Martin et al., 2010; Di Roberto et al., 2012; Nyland et al., 2013), so the glass signal in AND-2A is likely related to ice volume variations in southern East Antarctica. On this basis, sediments with more volcanic glass should be underlain by sediments with evidence for ice-sheet grounding, and be associated with (or perhaps overlie) diamictites with a southern provenance (particularly SM).

STRATIGRAPHIC UNITS

Five composite sequences are recognized in the lower part of the core, based on the stratigraphic nomenclature of Fielding et al. (2011, their table 2, Fig. 3). Each of these composite sequences is internally characterized by a consistent stratigraphic stacking pattern or vertical stratigraphic motif. CS1 comprises mainly diamictite; CS2 is dominated by interlaminated siltstone and sandstone, with less abundant sandstone and siltstone beds, and is largely devoid of diamictite; CS3 is dominated by diamictite with subordinate sandstone and minor mudstone; CS4 is distinguished by an abundance of siltstone over sandstone, with very little diamictite, and CS5 is a thick interval of diamictite-dominated lithologies with intercalated, less abundant sandstone and mudstone.

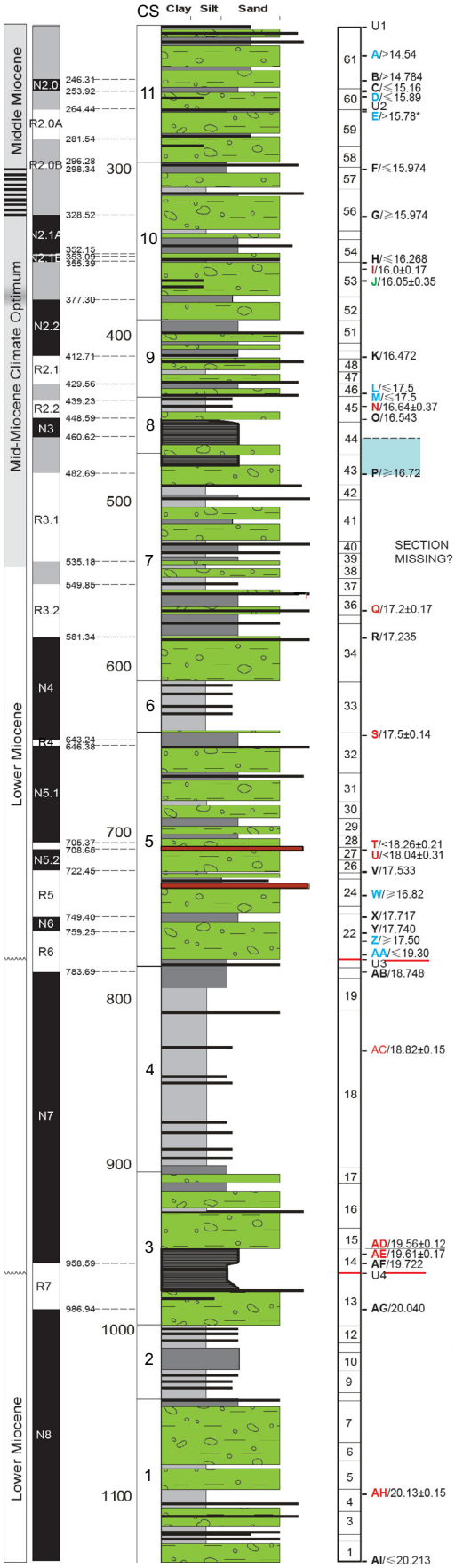

Figure 4. Age data and paleomagnetic reversals for the early and middle Miocene section in AND-2A based on SMS Science Team (2010), and the five composite sequences (CS, 1–5) described in this paper. See Levy et al. (2016; their supplementary material table 5.1, their figures S2 and S5) for details of chronostratigraphic data.

EARLY MIOCENE INTERVAL

Description of CS1 (1138.54–1042.55 m)

CS1 (Figs. 5 and 6) is ~96 m thick, and is dominated by diamictites, with units of sandstone and mudstone individually up to several meters thick that subdivide the CS into seven smaller-scale sequences (S1–S7; Fig. 3) on the basis of cyclical vertical stacking of lithofacies (Fielding et al., 2011). Each of these sequences is up to 20 m thick and each is defined by a distinctive, sharp to gradational base, overlying fine-grained sediments.

In general, the diamictites are black, clast-poor, sandy and stratified. Clasts comprise between 1 and 5% of the lithology and consist of angular to subrounded clasts up to 14 cm diameter. Wispy lamination, interbeds of siltstone with dispersed clasts, ~1-cm-thick siltstone to very fine-grained sandstone, and cm-thick interbedded diamictite and siltstone occur in several intervals with serpulid tubes and shell fragments present in places. Boxwork fractures, low-angle fractures cemented with brown-colored cement, and high-angle fractures filled with calcite occur in diamictites in the lower half of CS1.

Sequence 1 is likely incomplete, as drilling stopped before the base of the diamictite was reached. The drilled section of this sequence comprises ~10 m of mainly clast-poor, sandy diamictite with fragments of serpulid tubes and shells, high-angle fractures filled with carbonate cement, and boxwork fractures. This is overlain by cm-bedded sandstone, mm-interbedded siltstone, and very fine sandstone, with granules in places. Soft-sediment deformation and microfaults are also present. A 3-m-thick interval of bedded sandstone and mudstone at the top of Sequence 1 (Fig. 6) includes laminated mudstone, beds of grit and mudstone with isolated grit clasts. Sequence 2 diamictite is stratified, with clear evidence of dropstones within it as well as intervals of laminated siltstone, indicating cycles of deposition, and there are boxwork fractures near its base. The ~11-m-thick diamictite in Sequence 3 is similar to the thick diamictite of Sequence 1, but with strongly deformed stratification and calcite-cemented fractures in its basal part and is more stratified. No boxwork fractures were noted in the ~4-m-thick diamictite of Sequence 4. There is a 10-m-thick unit of muddy sandstone with dispersed clasts within Sequence 4 that has foresets and parallel lamination, and pebble conglomerate at its base. The unit fines upward, and the CIA decreases upward. The ~14-m-thick diamictite of Sequence 5 is mainly clast-poor and contains serpulid and shell fragments at 11 places within it, as well as boxwork fractures just above its sharp, loaded base. Sequence 6 has an ~10-m-thick stratified diamictite that is mainly clast-rich and sandy and has thin interbeds around 1070 m, suggesting at least two cycles within it. The sand at the top of this sequence has sand-filled veins and clastic intrusions. The ~19-m-thick diamictite of Sequence 7, at the top of CS1, is clast-poor, stratified and sandy, with wispy lamination, serpulid tubes and shell fragments. It is overlain by medium-coarse sandstone and convoluted beds of fine sandstone.

Finer-grained units occur near the tops of each of the seven sequences recognized in CS1. Lithologies include dm-thick intervals of black interstratified clayey siltstone, coarse siltstone and fine sandstone, interlaminated with mm-scale pinstripe lamination, cm-thick beds of gritty and very coarse-grained sandstone, mm-cm bedded well sorted sandstone and a unit of one centimeter amplitude foresets. Centimeter- to m-thick beds of black, fine to medium sandstone with dispersed clasts occur intercalated with the diamictites (particularly in the upper portion of CS1), along with silty fine sandstone with dispersed to common clasts that are angular to subangular and up to 10 cm in diameter. Sandstone units locally contain convolute bedding or planar stratification.

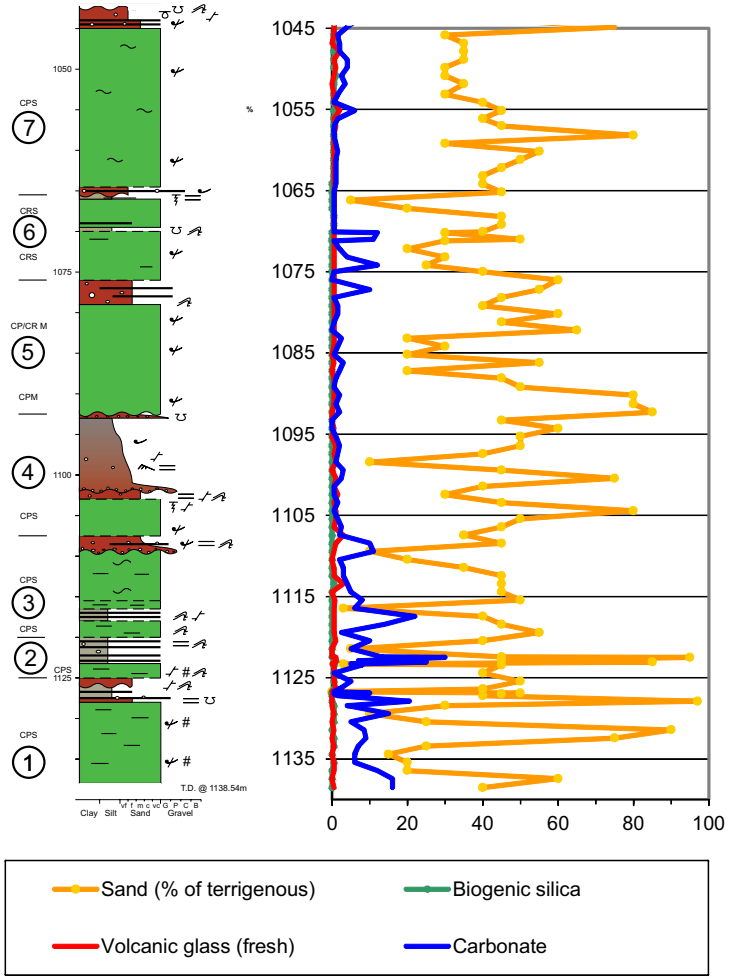

Figure 5. Composite Sequence 1 with smear slide data. See Figure 2 for a key to colors in the lithologic column and Figure 3B for graphics symbols. Abbreviations as in Figure 3 caption.

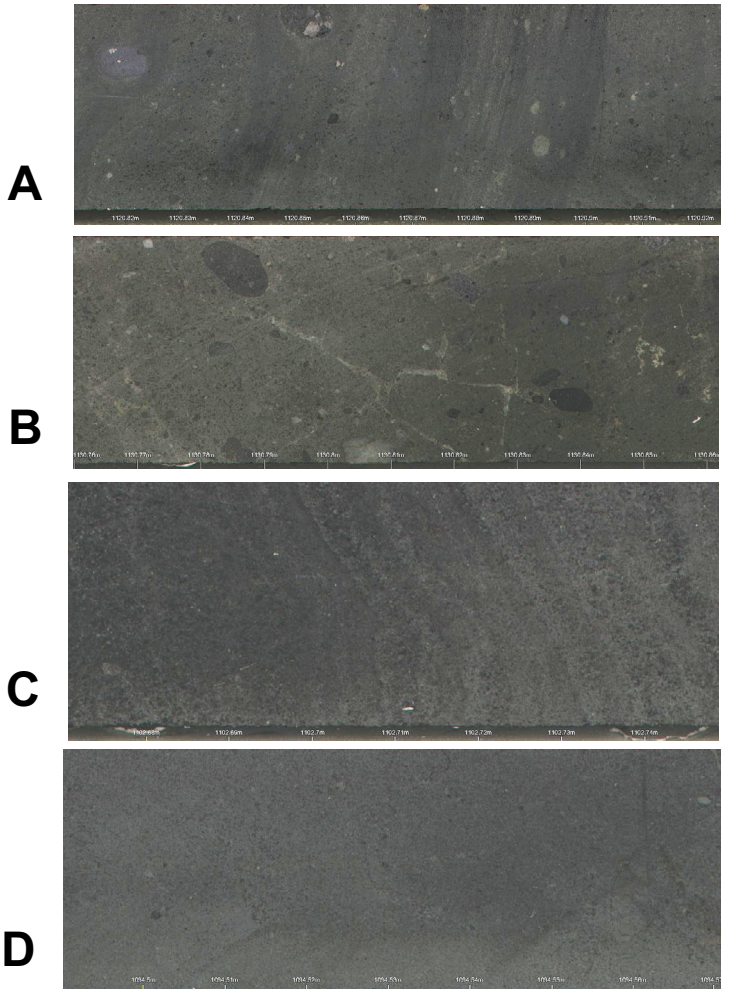

Figure 6. Composite Sequence 1 lithologies showing (A) stratified diamictite, (B) boxwork fractures, (C) laminated sandstone within a sandy interbed, (D) sandy mudstone with coarse sand grains.

Foraminifera and macrofossils such as an articulated bivalve or brachiopod shell and serpulid tubes occur sporadically throughout.

Coarse clasts (granule to pebble-cobble) have a local TAM/KB provenance, with sparse evidence of southern sources (SM) near the base of CS1, in sequences 1 and 2. Smear slides show almost no volcanic glass and very little biogenic silica (fragments of spicules, only near the base and top of CS1). Carbonate was noted in smear slides from all sequences in CS1, though it is more common near the base of CS1, where it occurs as micrite and as spar. Carbonate is in the form of serpulid tube and shell fragments and is more common than the 1-m-spaced smear slides indicate.

Interpretation of CS1

CS1 ranges in age from 20.2 to 20.1 Ma or older (Fielding et al., 2011). It is dominated by stratified diamictite, with interbedded laminated siltstone, dropstones, and marine macrofossils. The finer, sandy and silty upper parts of the component sequences are interpreted as the increasingly distal deposits of retreating ice, with rhythmic coarse-fine alternations of sediment arranged into regularly spaced "bundles") millimeter/pinstripe cyclicity most likely recording tidal pumping and possibly also seasonal control of sediment discharge. The 10-m-thick unit of muddy sandstone with dispersed clasts within Sequence 4 is interpreted as the deposit from outflow of a subglacial stream into standing water. The unit fines upward, consistent with either increasing distality (perhaps temporary glacial retreat) or reduced sediment supply (e.g., ice-bound due to cooler temperatures). The up-section lowering of the chemical index of alteration (CIA) at this level (Levy et al., 2016) favors the latter.

Coarse clasts have KB provenance, suggesting that sediment was derived from local glaciers that reached the coast and calved debris-laced icebergs. Increased carbonate percentage below S4 suggests conditions were warmer or ocean waters less corrosive than in the upper half of CS1, consistent with the generally lower CIA (Levy et al., 2016) and higher percentage of sand above Sequence 4 (Fig. 5). The boxwork fractures and low- and high-angle fractures below Sequence 4, indicating ice-grounding, are more likely due to grounding of icebergs than the presence of an ice sheet at the drill site, because of the ice-rafted material. The combined evidence points to a sub-polar climate, with perhaps cooler conditions during deposition of the upper half of CS1. The presence of clasts supplied by local glaciers indicates conditions were cool enough for local glaciers to have reached sea level but at times were warm enough for them to calve icebergs; shell material suggests more open marine settings at least intermittently.

The seven sequences distinguished in CS1 span perhaps 100 k.y. (certainly less than 200 k.y.; Fig. 4), suggesting they are unlikely to be obliquity-controlled, but might be precessional (19 or 23 k.y.) or sub-Milankovitch in frequency.

Description of CS2 (1042.55–996.69 m)

CS2 is ~46 m thick. The contact between CS1 and CS2 (at 1042.55 m) is indistinct at the millimeter scale but marks a change up-core from sandstone with dispersed clasts to diamictite. CS2 is dominated by sandstone, siltstone, and mudstone, commonly as mm-bedded rhythmites (Figs. 7 and 8). Diamictite, coarse, rainout ice rafted debris (IRD) and lonestones are present but form only a minor component. Millimeter-thick beds of silt alternating with mud-

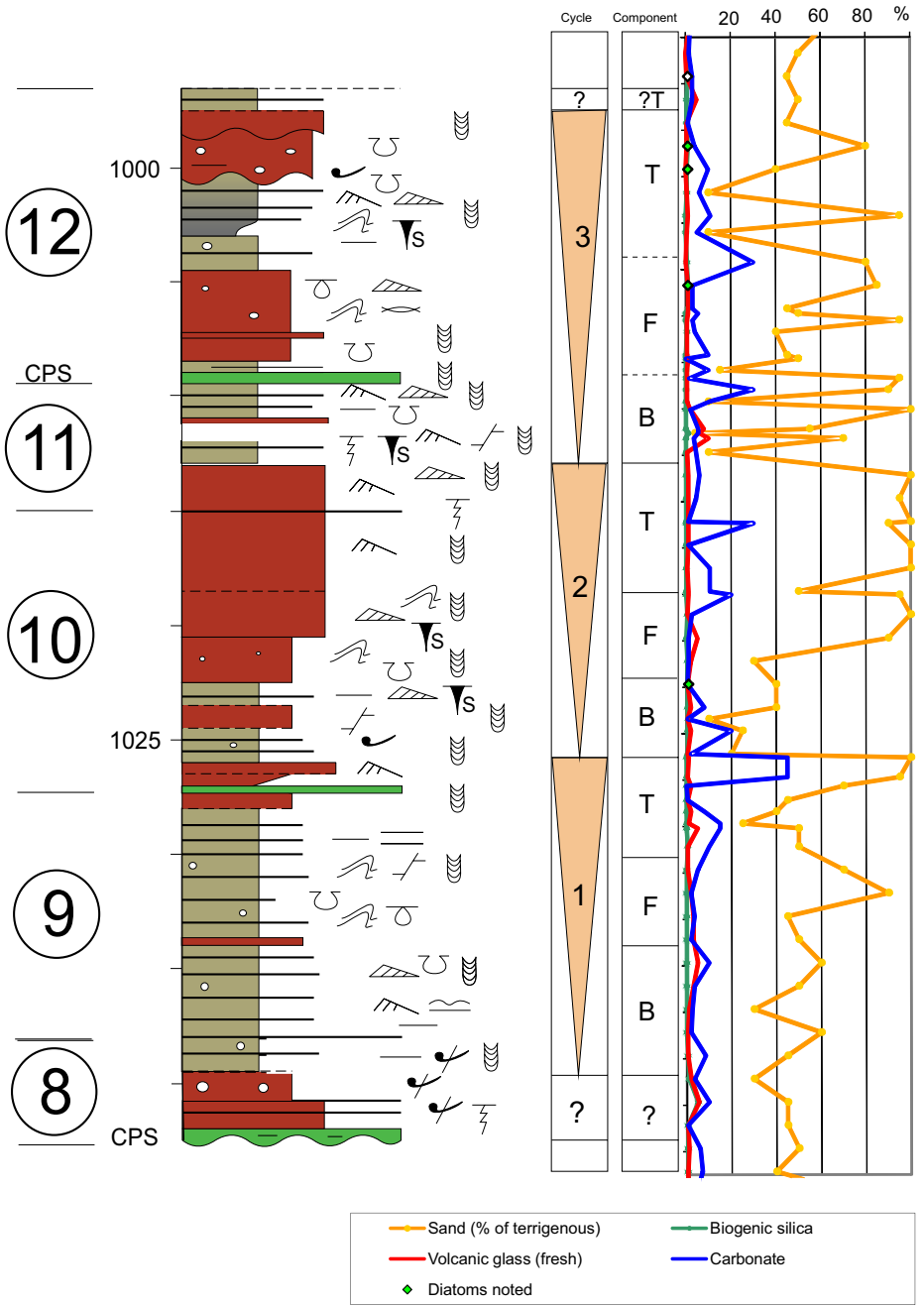

Figure 7. Composite Sequence 2 with smear slide data. See Figure 2 for a key to colors in the lithologic column and Figure 3B for graphics symbols. Abbreviation as in Figure 3 caption as well as T—delta top, B—delta base, F—delta front.

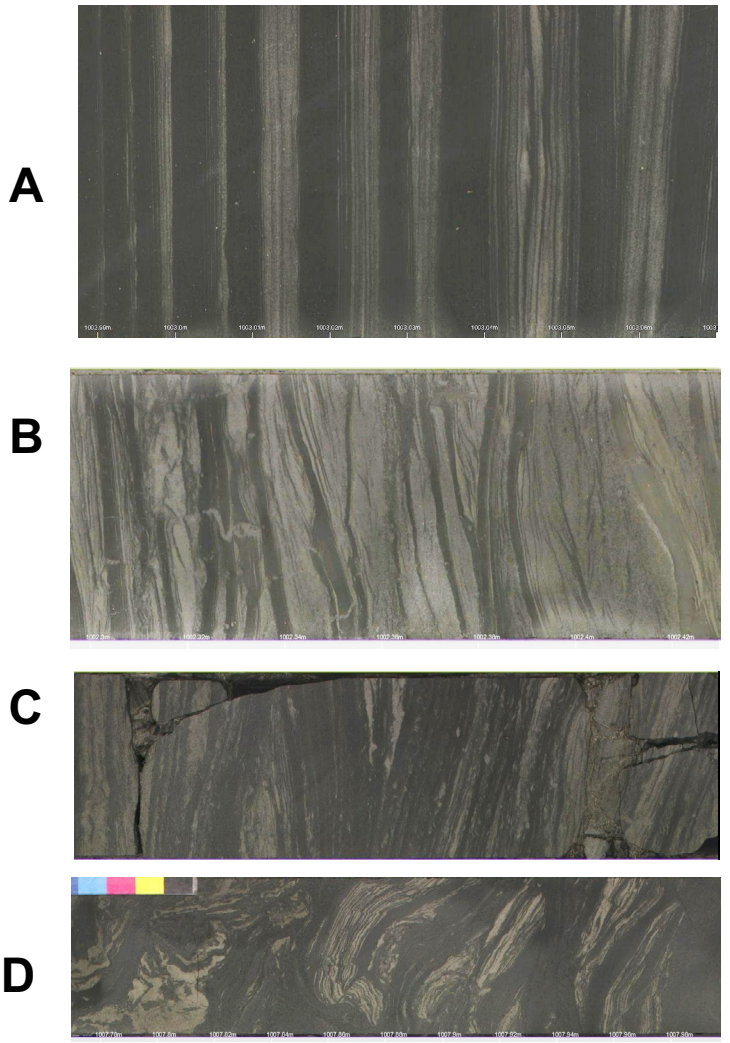

Figure 8. Composite Sequence 2 lithologies showing (A) mm-bedded rhythmites, (B) mud drape couplets, (C) scour, (D) soft sediment deformation.

stone commonly occur in bundles separated by thin beds of mudstone (some of which contain small dropstones). Some siltstone beds have graded tops while others have sharp tops and foresets. While most ripple foresets appear unidirectional, there are a few possibly bidirectional foresets, and mud-drape couplets occur (Fig. 8). Slump units are present in three zones in CS2, just below increases in sandstone content.

The sandstone component of the heterolithic lithologies is light gray to black, muddy and very fine- to fine-grained. The clasts are angular to subrounded, up to 8 cm in diameter and some occur in clusters. Sandstones are planar laminated, and ripple cross-laminated with mud drapes. Pinstripe lamination is prevalent in the most thinly laminated intervals. Tops and bases of sand-silt laminae are sharp or gradational and some of the thinnest are discontinuous, appearing starved suggesting current influence rather than pure fallout. Couplets and bundles of 5–7 and ~14 laminae, sometimes in foresets, occur commonly and bifurcating mud laminae occur in places. Centimeter-scale compensation bedding (Mutti and Sonnino, 1981; Slatt, 2013) indicates preservation of positive bedforms at the sediment-water interface, with little if any erosion, though locally centimeter amplitude scours filled with interlaminated sand and mud indicate the presence of erosive currents (Fig. 8). The mudstone locally has a bioturbation index (BI, following Bann and Fielding, 2004) of 2–3, with ichnofossils including *Teichichnus* and ?*Rhizocorallium* burrows.

There are three main intervals of soft-sediment deformation. In some intervals heterolithic interbeds have been physically intermixed by intensive soft-sediment deformation (Figs. 7 and 8). Cracks seen in cross section and inferred to result from synaeresis are common in some intervals. The sandstones are bioturbated (BI = 2–3), and include serpulid tubes concentrated into clusters. Nodular pyrite cement is common in some intervals.

The other main lithology is sandstone in cm- to m-thick beds, which tend to be less abundant in the lower part of the CS. These sandstones are very fine- to fine-grained, contain dispersed clasts, and are light gray, gray, to black in color. Dispersed clasts are generally rare, angular to subrounded in shape and up to 4 cm in diameter. Clasts are generally polymict and include intraformational mud clasts and some angular diamictite clasts. Ripple cross-lamination in 1-cm-thick sets is locally common, and some include mud drapes. Possible bidirectional ripples occur locally and black grains, perhaps volcanic, are present on some ripple foresets. Bioturbation is common throughout (BI = 4–5), and includes ?*Planolites*.

Two beds of cm- to dm-thick, black, clast-rich sandy diamictite occur. The clasts are predominantly granule-grade, with intraformational clasts becoming more common below 1008.90 m. Coarse clasts in the top few meters of CS2 have a local KB affinity (Talarico and Sandroni, 2011).

Interpretation of CS2

CS2 ranges in age from 20.05 to 20.1 Ma (Fielding et al., 2011). It is dominated by sandstone, siltstone, and mudstone, commonly in mm-bedded rhythmites, in marked contrast to the ice-influenced sediments of CS1. IRD including isolated dropstones are only a minor component but their presence indicates that ice shelf or marine-based glaciers were present in the region, but they were likely small or distal from the deposition site.

We recognize three main sedimentary cycles in CS2 (labeled 1–3 in Fig. 7) and interpret these as deltaic and estuarine in origin. Each cycle has a middle

interval with increased evidence for slumping, consistent with loading in delta front slope settings, and sandy, potential delta top sediments that occasionally include thin conglomerates. The sandy, basal part of CS2 (1040–1044 m) lies below the lowest cycle and, given the units of diamictite within it, is interpreted to record glacial melt and early stages of ice retreat. Cycle 3 appears to record a shallower setting (perhaps due to reduced accommodation), with possible delta top sands overlain above 1007 m by tidally influenced probable estuarine sediments capped at a transgressive ravinement surface at 1000.48 m (Fielding et al., 2011). The base of a fourth cycle might be present above 997.5 m, truncated by glacial erosion at the base of CS3. The age range for CS2 is ca. 50–60 ka (Fig. 4), suggesting the cyclicity is at a precessional (21 k.y.) or sub-Milankovitch frequency.

The mud-drape couplets (Fig. 8B) are interpreted as paired ebb tide slack-water deposits (Visser, 1980; Fenies et al., 1999). Cowan et al. (1997, 1998) noted annual couplets in glacimarine settings, and Cowan and Powell (1990) described two couplets produced each day by semidiurnal tides where sediment supply from meltwater plumes was tidally controlled, though the AND-2A couplets are thinner and generally finer-grained than both these examples. Bundles of ~2–14 laminae in AND-2A can be interpreted as diurnal, weekly, and perhaps semi-lunar cycles. Centimeter-amplitude scours filled with interlaminated sand and mud indicate intermittent stronger currents, perhaps associated with storm events.

Rippled coarse-grained laminae occur in glacilacustrine settings fed by hyperpycnal underflows, particularly on lower delta foreslopes, but are reportedly absent in glacimarine settings, where densities of sediment-laden discharges are rarely sufficient to cause underflow transport and deposition (Ó Cofaigh and Dowdeswell, 2001). However, the presence of marine microfossils in CS2 demonstrates a marine setting. We infer that the rippled sandstones were not deposited from periglacial sediment plumes but rather in an ice-distal shallow-marine setting. CIA data indicate weathering in a more humid climate than in CS1 and CS3 (Levy et al., 2016).

Units of typically mm-thick beds of siltstone alternating with clay-rich mudstone are interpreted as bottom sets of deltas. The laminae commonly occur in bundles separated by thin beds of mudstone. Some of the thin mudstone beds contain small dropstones, suggesting they are seasonally controlled annual varves. Some silt beds have normally graded tops, consistent with settling from sediment plumes, while others have sharp tops and foresets indicating modification by bottom currents. Laminae thicknesses are generally at the thin end of the 0.2–1 cm range typical of glacimarine settings (Ó Cofaigh and Dowdeswell, 2001). This might be due to low-salinity conditions (causing less flocculation) likely within surface waters of the paleo–Ross Sea embayment allowing longer transport distances and hence thinner laminae. Modern plume deposits mostly occur within several tens of kilometers from the ice front (Elverhøi, 1984; Pfirman and Solheim, 1989; Syvitski, 1989; Lemmen, 1990; Wang and Hesse, 1996; Dowdeswell et al., 1998). The drill site is currently within a few tens of kilometers from termini of major modern grounded-ice glaciers (e.g., the Koettlitz and Blue glaciers) to the east in the TAM, and ~1000 km from the modern southern margin of the Ross Sea, and we suggest that sediment plumes came from glaciers off the TAM or that the southern ice sheet front was well out into the paleo–Ross Sea in the early Miocene. An attempt to compare grain size distributions of the silt laminae with those of aeolian sediment proved inconclusive due to masking by halite (Field and Atkins, 2012), so we are unable to distinguish whether the silt was purely current-sorted, or aeolian material that had been sorted and transported while settling through the water column.

Soft sediment deformation is unlikely to have been caused by ice loading because evidence for glacial ice over the site is lacking. We infer instead that there was a paleoslope sufficient to promote slumping. This is consistent with inferred high sedimentation rates in a delta. Slump units indicate a significant paleoslope in three stratigraphic zones in CS2, each occurring just below increases in sand, suggesting there are cycles present.

CS2 was built from sediment supplied by drawdown (after Smith et al., 1990) and laterally sourced overflow plumes, with sandier sediments outboard of a source of fluvial sediment (Fig. 6). Bottom currents locally reworked fine silt laminae. The drill site was unlikely to have been proximal to the ice front (as in fjord-head deltas; e.g., Dowdeswell et al., 1998) as the sediments lack significant diamictites and they are unlikely to be shelf break, trough-mouth fans (Vorren and Laberg, 1997) because they do not contain proximal till delta deposits; also, seismic lines do not show shelf-edge morphology at this stratigraphic level. The sediments are generally well sorted, consistent with the absence of sediment rain from floating ice, but the occasional presence of dropstones and IRD indicates glacial influence (with icebergs) nearby on a mixed, fluvioglacial margin. Preservation of the succession and facies repetition suggest accommodation increased, with either cyclic sediment supply or cyclic relative sea-level changes.

In an alternative model, Fielding et al. (2011) distinguished five sequences within CS2, following criteria applied consistently throughout the core and based primarily on abrupt, up-core coarsening of sediments marking sequence boundaries, with sequence development caused by advance and retreat of glaciers. Three beds with >1% pebbles (i.e., diamictite) and two of pebble conglomerate were logged in CS2, requiring subdivision into five sequences (Fig. 7):

(1) S8 comprises diamictite and sandstones (lowstand) overlain by mudstone (highstand);
(2) S9 has a thin basal conglomerate (lowstand), but is dominated by mudstone (highstand delta toe and delta front), with sandstone at its top;
(3) S10 has a thin basal diamictite with overlying sandstone (lowstand), overlain by highstand mudstone and sandstone;
(4) S11 has a thin basal conglomerate overlain by sandstone (lowstand) overlain by mudstone; and
(5) S12 is more varied in character with a basal conglomerate overlain by mudstone and delta front sandstone, overlain by more mudstone, sandstone and mudstone.

However, CS2 contains facies and stacking patterns not found in the rest of the core, suggesting a different approach to this five-sequence model is required. In the three-cycle model suggested here (labeled 1–3 in Fig. 7), units of coarser grain size do not consistently mark sequence boundaries, and thin units with >1% pebbles, texturally classed as diamictite, could be delta-front debris flows or delta-top deposits not necessarily associated with sequence boundaries in this CS.

There is little evidence for ice-transported coarse-grained sediment in CS2 and this is interpreted to record significantly more ice-distal conditions than CS1. An alternative interpretation, that ice proximity was the same as for CS1 but that glaciers had shifted laterally away from the drill site rather than retreating, is rejected because: (1) the basal part of CS2 has more sandstone beds, and diamictite beds are thinner, suggesting glacial retreat; and (2) the upper part of CS2 has units that lack lonestones, suggesting there were periods with no ice-rafting of clasts larger than sand grains, and hence a decrease in ice-calving.

Nevertheless, the presence of some coarse, ice-rafted clasts of SM provenance at the top of CS2 might record renewed ice-calving in the south.

Description of CS3 (996.69–901.54 m)

The boundary between CS3 and the underlying CS2 is not preserved as it coincides with a curatorial sawcut at 996.69 m but is at the apparently abrupt contact between clast-poor, sandy diamictite and underlying poorly sorted sandstone. CS3 is 95 m thick and is dominated by clast-rich and clast-poor diamictite with subordinate sandstone and minor mudstone (Fig. 9). An age of 19.9–19.4 Ma is inferred (after Fielding et al., 2011).

Five sequences are distinguished (Fielding et al., 2011). The lowest two (13 and 14) and top (17) sequences are sand-rich but the middle two (15 and 16) are more mud-dominated; clasts occur throughout all five sequences. The sequences have a lower interval of diamictite, and sand- to silt-dominated upper parts, except for Sequence 14, which lacks diamictite and comprises a basal conglomerate with shell fragments; these pass up into shelly sandstone and siltstone that locally has foresets and bioturbation (Figs. 9 and 10).

Diamictites are very dark gray and have clast abundances between 5% and 7.5%, with angular to well-rounded polymict clasts up to 4 cm diameter. The clast-poor variants contain 1%–5%, angular to subrounded polymict clasts up to 15 cm diameter. Clast-poor diamictite in places grades upward into clast-rich diamictite. Crude stratification at cm- to dm-scale is evident in both styles of diamictite, produced from the alignment of elongate clasts, silt-rich laminae, matrix grain-size variations, or alignment of shell fragments (including serpulid shells). Shear and boxwork fabrics occur in unstratified diamictite near the middle of the unit and near the base, and Passchier et al. (2011) noted evidence for ice-grounding at ~906 m near the top of CS3.

Mudstones are less common than diamictite and sandstone. They are very dark gray sandy mudstones (siltstone) with dispersed clasts forming

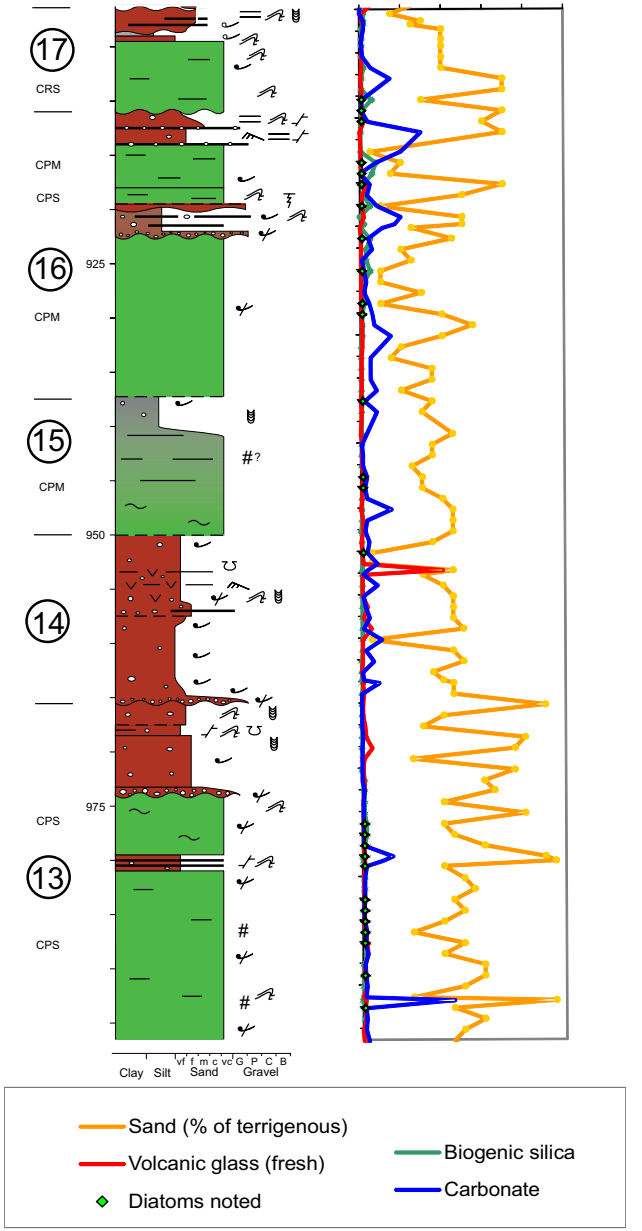

Figure 9. Composite Sequence 3 with smear slide data. See Figure 2 for a key to colors in the lithologic column and Figure 3B for graphics symbols. Abbreviations as in Figure 3 caption.

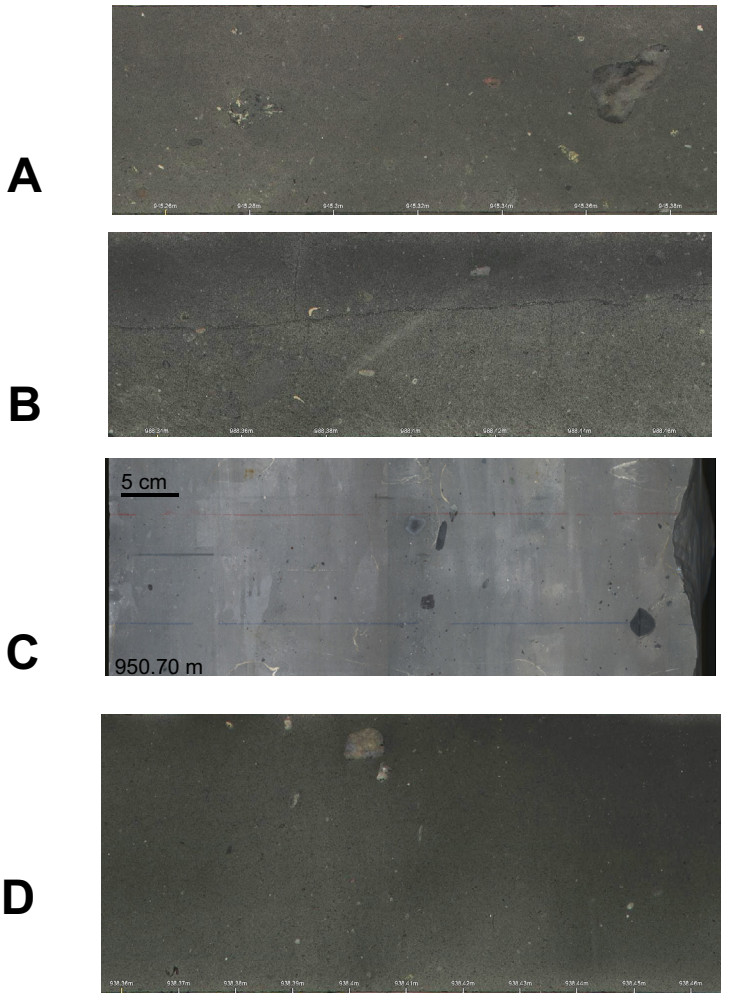

Figure 10. Composite Sequence 3 lithologies showing (A) diamictite, (B) boxwork fractures, (C) unwrapped whole core image of shells in sandstone (950.70–951.22 m), (D) mudstone with dispersed clasts.

beds up to ~2–40-cm-thick. Clasts are angular to subangular, polymictic, and up to 7 cm in diameter. Mudstone is typically interbedded with ~10 cm ranging up to >100 cm thick beds of sandstone with dispersed clasts or cm-scale stratification.

About a quarter of CS3 is sandstone and most of this is in Sequence 14. Most of the sandstone beds are very dark gray in color, muddy (silty) sandstone with angular to well-rounded dispersed clasts. The latter are up to 7 cm in diameter and are polymict in composition. Pumice clasts are locally abundant and volcanic glass reaches 40% in some smear slides. Sandstones range from fine- to coarse-grained. Millimeter-scale stratification appears to be produced from interlaminated coarse-grained and fine-grained sandstone and cm-scale lamination by interbedded fine-grained sandstone, often with soft-sediment deformation features. Bioturbation (BI = 3–4) is present and shells, especially serpulids, are common in the sandstones. Thin sandy conglomerate is present in places.

CS3 contains coarse clasts with southern provenance and none from the local (KB) region present below this level in the core (Talarico and Sandroni, 2011). Additional, distal southern provenance (CB region) is indicated in the top two diamictite units of CS3 and one in the middle (in Sequence 15). Flame structures and probable loading occur, and soft sediment deformation is common, suggesting high rates of deposition. The top half of CS3 contains the highest percentages of dolerite clasts in the examined core section, and a much higher percentage of clasts of intrusives than the lower half, in which the coarse clast population is dominated by clasts of volcanics with McMurdo Volcanic Group affinities, inferred to be from the Mount Morning eruptive center (Panter et al., 2008; Talarico and Sandroni, 2011; Nyland et al., 2013). Smear slides indicate biogenic silica and carbonate (micrite and spar of uncertain origin) have generally higher percentages in the top two sequences.

Interpretation of CS3

Levy et al. (2016) infer a major, erosional unconformity is present within the ~25 m interval of sandstone comprising Sequence 14, at 965.43 m. It is unlikely that the sandstone interval was deposited sub-glacially because of the presence of shell material and bioturbation in Sequence 14. The higher percentage of sand below the inferred unconformity is consistent with lower CIA values (Fig. 9), though TEX_{86} values suggest warmer conditions just below the unconformity (Levy et al., 2016); the increased carbonate above the inferred unconformity suggests warmer conditions than below, consistent with the higher CIA values recorded.

The dominance of diamictite at the base and in the upper half of CS3 (Fielding et al., 2008), with grounded ice indicated by fractures and boxwork fabrics, implies ice advance relative to the underlying CS2, or at least more frequent presence of icebergs. CS3 contains clasts from southern sources, not local TAM glaciers. The latter could have been held back by larger glaciers from the south as proposed by Talarico and Sandroni (2011; Fig. 3A), or TAM glaciers might not have been large enough to reach the coast and supply ice-trapped debris to the Ross Sea region, with the presence of clasts derived from the south reflecting greater calving of southern glaciers (Levy et al., 2016).

The high percentage of volcanic clasts in the lower half of CS3 probably records renewed erosion of the Mount Morning volcanic center by southern glaciers (SM provenance) following a probable reduction in ice cover during CS2 time (which we infer was a relatively warm period). The percentages of

volcanic glass are low (suggesting no major eruptions occurred) except in the upper part of Sequence 14, post-dating and consistent with crustal unloading at the inferred, regional erosional unconformity.

The five sequences span around 500 k.y., suggesting 100 k.y. eccentricity control, not allowing for any significant unconformities.

Description of CS4 (901.54–778.34 m)

CS4 is quite unlike the other compound sequences as it is dominated by siltstone and sandstone, with very little diamictite (Figs. 11 and 12). The lower boundary is the irregular (probably loaded) contact between clast-rich, sandy diamictite (CS4) and poorly sorted gritty sandstone (CS3) at 901.54 m. CS4 comprises mainly black to greenish-gray sandy siltstone with dispersed angular to subangular polymictic clasts up to 6 cm diameter, some of which have deformed laminae beneath them. Intermittently, the sandy siltstone is interbedded with black clayey siltstone with dispersed clasts up to 1 cm diameter. Clayey siltstone units are generally internally stratified, locally with well-developed laminae. There are also cm- to dm-thick units of millimeter bedding with no clasts coarser than sand grade. Remnants of mm-thick bedding of mainly silt and mud are discernible in places and might have been common prior to bioturbation. *Chrondrites* burrows occur in clayey siltstone units. Overall, the lower two-thirds of CS4 (901.54–822 m) is similar to CS2 in being essentially fine-grained and having intervals of cyclic lamination. However, CS4 has less sandstone than CS2 and is not as clearly cyclic.

There is an overall facies change around 822 m, between the top third and lower two-thirds of CS4. Below 822 m, mm-scale bedding, spherical well-rounded pebbles, ripple foresets, slumped bedding, burrows, and biogenic silica and carbonate are much more common than above this depth (Fig. 9); above it, most shell material is broken. There are possible up-section increases in sand content based on smear slides from 856–843 m and 840–825 m, and these coincide with increases in biogenic silica, and there is an up-section decrease in sand content from within the top part of CS3–885 m in CS4. Biogenic silica peaks occur around 850 m and around 827 m. Burrowing is generally more common and bedding is less well defined than in CS2. Dispersed granules, in units with no pebbles or cobbles, occur throughout CS4, but are more common above 822 m.

Bedding orientations derived from whole-core photographs oriented using image log data indicate a dominant dip to the north-northwest around 896 m (Fig. 11). Sedimentary structures with easterly and southerly dips occur around 882–885 m in sandy mudstone with sparse granules and remnants of mm-bedding. Dip magnitudes increase up-section by ~30°. If these dips are restored using the northerly dips below them, they swing slightly to the east-southeast. Dips near the base of CS4 are more to the north and northeast.

Talarico and Sandroni (2011) noted the percentage of sedimentary intrabasinal pebbles is higher in most of the upper part of CS4, reaching up to >20% (interval ~808–790 m) compared to <5% below 808 m. Their provenance studies reveal potentially four phases of pebble derivation in this part of the core, though low numbers of basement clasts make the interpretation below equivocal. In the top of CS3 to the lowest quarter of CS4 (~905 to ~872 m), clasts were derived from local, TAM sources lying to the southwest/west of the drill site (KB region) plus southern sources (SM region), with an upward decrease in pebble abundance. Above this, from ~872 to ~837 m, in a less lithologically diverse interval dominated by siltstone, the source was SM, with no local TAM sources. Above this is an interval with KB/local TAM clasts but no southern sourced clasts, from ~837 to 807 m; this interval contains the last occurrence of KB clasts till at least 100 m farther up-core, well into CS5 (and over 1 Ma younger). In the top quarter (above ~807 m) the source of pebbles was solely southern (SM). Well-rounded, high-sphericity pebbles occur at several levels in CS4, all within or near intervals of SM provenance.

At 791 m there is a sandstone unit with angular intraclasts above an irregular base. The sandstone is mainly parallel laminated, with strong soft-sediment deformation. Divergent and convex-upward laminae suggestive of hummocky cross-stratification (HCS) were noted around 788.6 m. There are carbonaceous clasts just below 786 m.

Interpretation of CS4

An age range from 19.4 to 18.7 Ma has been assigned to CS4. While CS4 is dominated by mudstone rather than diamictite, the dispersed granule to cobble clasts suggest the drill site was influenced frequently by ice. Highly spherical, very well-rounded pebbles are rare but their presence at several levels suggests a supply of water-rounded clasts, perhaps from sub-glacial streams of wet-based glaciers (probably in the SM region), assuming they have not been reworked. Laminae of poorly sorted sediment could have been produced as IRD during seasonal sea-ice melting, releasing accumulated aeolian sediment transported by variable winter winds. The mm-scale bedding of silt without granules suggests sediment plume transport and its cyclicity suggests seasonal or tidal influence, perhaps through pumping of tidewater glaciers. Fine-scale bedding is indicated by poorly preserved remnants of bedding, with cryptic to good evidence of bioturbation. Soft sediment slumping suggests a significant depositional slope was present at least locally at times.

Dispersed granules in units with no pebbles or cobbles could be lag deposits transported during periods of strong bottom current activity (though the sparseness of foresets is not consistent with this), or comprise sediment transported by wind over sea ice and settling as fine IRD during summer breakout. Modern aeolian sediment on the Ross Ice Shelf is typically fine sand, but does locally contain coarse sand and granules within a few kilometers of land (Chewings et al., 2011). The drill site is currently many tens of kilometers from land but the early Miocene paleogeography of the area is not well constrained.

The upward decrease in pebble abundance noted by Talarico and Sandroni (2011) in the lower part of CS4 coincides with an interval of low sand content, and has CIA values suggestive of warmer conditions, which taken together

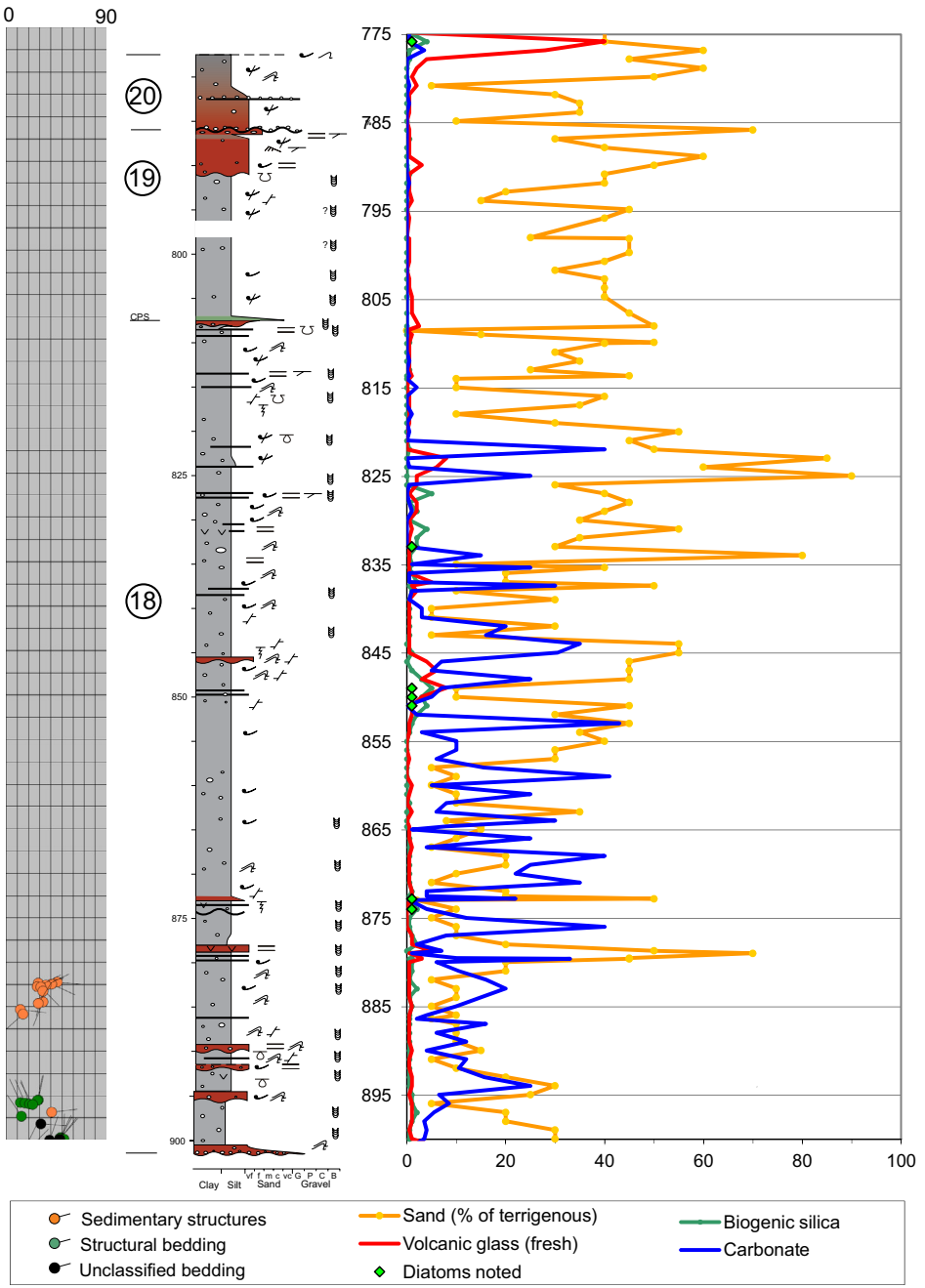

Figure 11. Composite Sequence 4 with paleocurrent dip directions from image log data (left), and smear slide data (right). See Figure 2 for a key to colors in the lithologic column and Figure 3B for graphics symbols. Abbreviations as in Figure 3 caption.

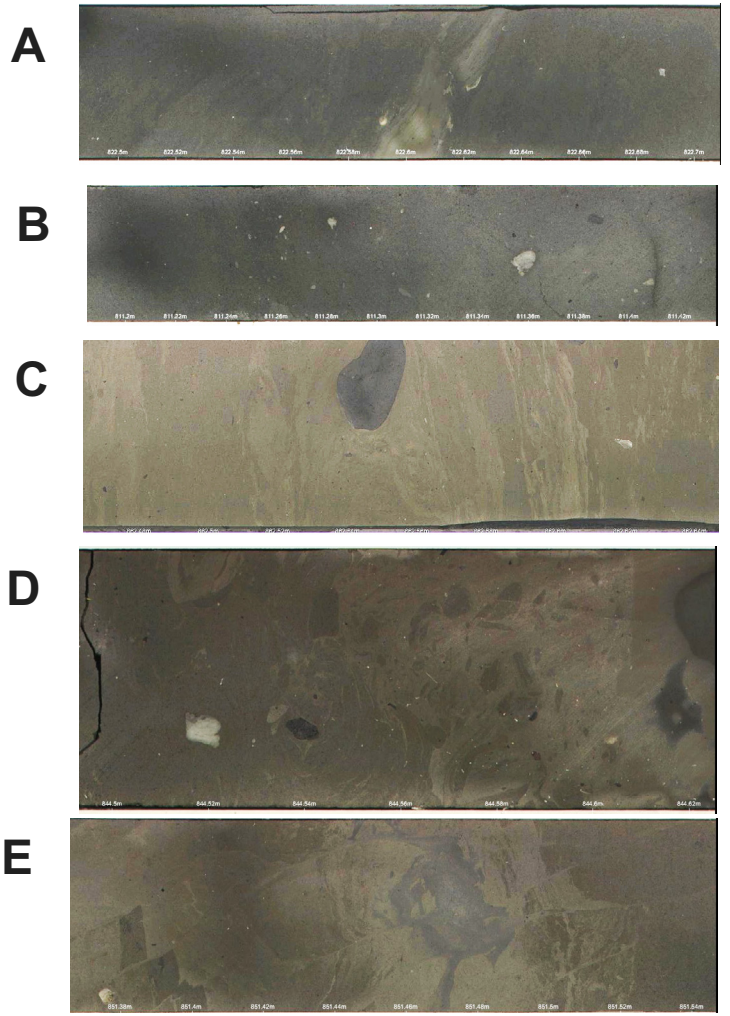

Figure 12. Composite Sequence 4 lithologies showing (A) typical mudstone lithology, (B) mudstone with fine, probable rain-out clasts, (C) mudstone with mm-bedding and rounded lonestone, (D) deformed, laminated mudstone, with fine lonestones, (E) mudstone with probably early formed fractures. Paleocurrent directions are based on borehole televiewer (BHTV) image data.

implies ice retreat. SM clasts return in the top quarter of CS4 (but without local TAM clasts), along with higher sand content and CIA values indicative of cooler conditions; this likely records renewed glacial activity in the south (eroding and releasing berg-rafted SM clasts), with local TAM glaciers land-locked behind the coastline.

The lower percentages of carbonate and biogenic silica in the top third of CS4 might result from less sunlight beneath sea ice or perhaps an ice shelf. The decreases are unlikely to result from dilution due to higher sedimentation rates, as the carbonate and silica components do not vary with sand content. The biogenic silica peaks around 850 m and 827 m are unlikely to be related to lowered sediment dilution as these increases coincide with increases in sand content. Broken shells above 823 m suggest reworking and transport of macrofossils and hence higher energy conditions. The sandstone at 791 m, near the top of CS4, is inferred to be channel fill, and this, along with the possible HCS and the broken shell material, indicate locally strong bottom currents, consistent with deposition above storm wave base during at least seasonal loss of sea ice.

Organic carbon material in clasts just below 786 m potentially records terrestrial conditions warm enough for plant growth, although it is not known if the clasts were derived from penecontemporaneous settings or were reworked from older sediments. Paleocurrent data indicate the depositional slope during early CS4 time (at least), dipped to the northeast and there were likely contour/bottom currents flowing toward the east. Pebble provenance at the base of CS4 is from the KB-SM regions and consistent with the paleocurrent data, provided a clockwise gyre existed, bringing icebergs northward from KB-SM then eastward to the drill site. The younger directions around 883 m in finer sediments include near-orthogonal currents which are presumed to be slope-parallel contour currents.

We infer a change from glacially variable conditions of CS3 to no grounded ice at the drill site in CS4, and gradual locking up of the sediment supply. There was perhaps only sea ice near the drill site (lower two-thirds of CS4) to mainly ice shelf or sea ice above ~822 m. The strong currents inferred from the preserved top 13 m of CS4 suggest more open conditions. The record between the top of CS4 and base of CS5 is inferred to be missing, truncated at an unconformity at the base of CS5.

The three cycles in CS4 span potentially 700 k.y. There are two age determinations in the interval, the top of magnetozone N7 (18.787 Ma) near the top of CS4, and an Ar-Ar date of 18.82 ± 0.15 Ma just above the middle of CS4. If a constant sedimentation rate is assumed then CS4 would record about 60 k.y., and this would be consistent with precessional cycles of about 20 k.y.

Description of CS5 (778.34–637.96 m)

The boundary between CS5 and the underlying CS4 is taken at the base of a thin diamictite at the base of S21, at 778.34 m. This assignment differs from that of Fielding et al. (2011), who placed it at the top of S21 (774.94 m) based on facies changes and the change upwards to thick diamictite at the base of S22 (Fig. 13). Our revision is based primarily on the marked increase in volcanic glass and volcanic clasts recorded around this level (Figs. 2 and 13), on the basis that the major unconformity inferred from age data around this level would then have immediately preceded the increase in volcanism,

perhaps triggered by unloading of sediment and ice cover. Franke and Ehrmann (2010) recorded an anomalously large increase in smectite and decrease in both illite and the quartz/clay ratio in sandstone just above 788 m, consistent with increased sediment supply from the McMurdo Volcanic Group (Franke and Ehrmann, 2010). Well logs provide some evidence for a change in lithologic composition around 778 m, with distinct up-well lowering of the baseline of natural gamma ray readings and an up-well increase in the K/U baseline (Hunze et al., 2013, their figs. 3 and 6). However, the density curve does not show a clear change in baseline for 20 m around this level, as could be expected if erosion had led to a contrast in burial compaction across the unconformity. The position of the unconformity is not certain, and further revisions may be warranted.

CS5 comprises mainly diamictite-dominated lithologies with intercalated, less abundant sandstone and mudstone (Figs. 13 and 14). The dominant lithology—very dark greenish-gray, mostly clast-poor sandy diamictite—has a sand content locally approaching 90%. Clasts are angular to well rounded, up to 14 cm in diameter and polymict. In general, the diamictite is interbedded with laminated sandstone or mudstone, or wispy laminae, often displaying extensive soft-sediment deformation and shearing. Boxwork fractures occur in places. Foraminifer, serpulid tubes and shell fragments occur sporadically throughout (Fig. 14B). Bases of diamictite units are typically gradational into underlying lithologies. In many places, the proportion of clasts drops below 1% and the lithology grades to muddy sandstone with dispersed clasts.

Finer grained lithologies include sandstones and mudstones. Sandstones are the more common lithology and comprise very dark greenish gray, muddy, very fine- to medium- grained sandstone with dispersed clasts, in part interbedded with muddy sandy conglomerate. Stratification, where present in the sandstone, occurs as mm- to cm-scale planar and inclined bedding, trough cross-lamination, or ripple cross-lamination. Small load casts are present at the base of some sandstone laminae. Possible bioturbation occurs in the lower portion of the unit, but is somewhat enigmatic (BI = 1–2). Many sandstone beds are disturbed by soft-sediment deformation. Smear slides indicate ~10% carbonate in the upper part, but >30% carbonate below 730.5 m, and up to 30% volcanic glass (Panter et al., 2008; Nyland et al., 2013). Discrete beds of intraformational granule to small pebble clast conglomerate are present. Serpulid fossils are rare in the sandstone, and the interval from 753.55 to 753.96 m contains biosilica. Sandstones also occur associated with siltstone beds and most grade upward into siltstone, though inverse grading also occurs. The siltstone is greenish black in color, displays mm-scale laminations, ripple cross-lamination, and soft-sediment deformation.

Mudstones comprise three dominant lithologies:

(1) Serpulid and shell-bearing, very dark greenish gray sandy mudstone with dispersed angular to rounded clasts up to 1 cm diameter. These are planar laminated at cm-scale with interbedded fine-grained sandstone, massive sandstone, and siltstone. Soft-sediment deformation is common.

(2) Very dark gray, fine- to coarse-grained siltstone, bedded at a mm-scale and locally microloaded. They form inversely graded beds up to 6 cm thick.

(3) Very dark greenish gray sandy crudely stratified mudstone (siltstone) with dispersed clasts up to 4 mm diameter. They are extensively modified by soft-sediment deformation and boudinage (folding and faulting).

Pebble provenance studies record mainly SM compositions, with a few CB clasts near the base (Talarico and Sandroni, 2011), and a local KB signal in the ~700–685 m interval (Sandroni and Talarico, 2011).

Interpretation of CS5

CS5 is dated as 17.8–17.35 Ma and marks a prolonged return (above Sequence 21) to diamictite-dominated lithologies. The presence in CS5 of macrofossils, unbroken diatoms, m-thick sandstone units (locally with ripple foresets) suggests periods of open water. CS5 shows much more variability in composition and facies than CS4, suggesting less stable paleoenvironmental conditions at the drill site.

The basal sequence (21) differs from sediments below in having pebbles, diatoms and other biogenic silica and volcanic glass; all these features are characteristic of CS5. The biogenic silica suggests more open marine conditions than in CS4 and the presence of pebbles in S21 indicates ice melt and rafting resumed at this time. The increase in volcanic glass might signal unloading of the crust in the Mount Morning area following loss of ice (following Nyland et al., 2013). This could have occurred during the time-gap around CS4 to CS5 time inferred from the age model and would be consistent with the base of Sequence 21 being unconformable.

The dominant unstratified diamictite lithology and presence locally of boxwork fractures indicates glaciers or icebergs reached the drill site and were transporting pebbles from southern regions (SM, CB). However, the diamictites are clast-poor, indicating either low erosive power or the erosion of non-basement, sediment-rich substrates, or that the clasts were transported by icebergs that were either infrequent or calved from marine-based glaciers. More local sources such as the TAM (KB) were able to provide clasts to the drill site only in the upper part of the CS. The intervals comprising fossiliferous sandstone and mudstone are inferred to indicate periods of relative ice retreat. The rounded clasts in mudstones might be sub-glacial stream debris, but these could have been entrapped by ice and rafted into periglacial marine settings and do not in themselves indicate glaciers near the drill site.

Twelve sequences have been distinguished in CS5. Delineation of the sequence boundaries has depended partly on the recognition of sedimentary indicators of basinward shifts in facies, and hence on the preservation of such indicators. There are ~15 units classified as diamictite in CS5 and it is possible there were more than 12, fifth-order changes in relative sea level, or episodes of ice advance and retreat, during the about 450+ k.y. period inferred for the age span of CS5. Nevertheless, the best estimates of cycle numbers and age

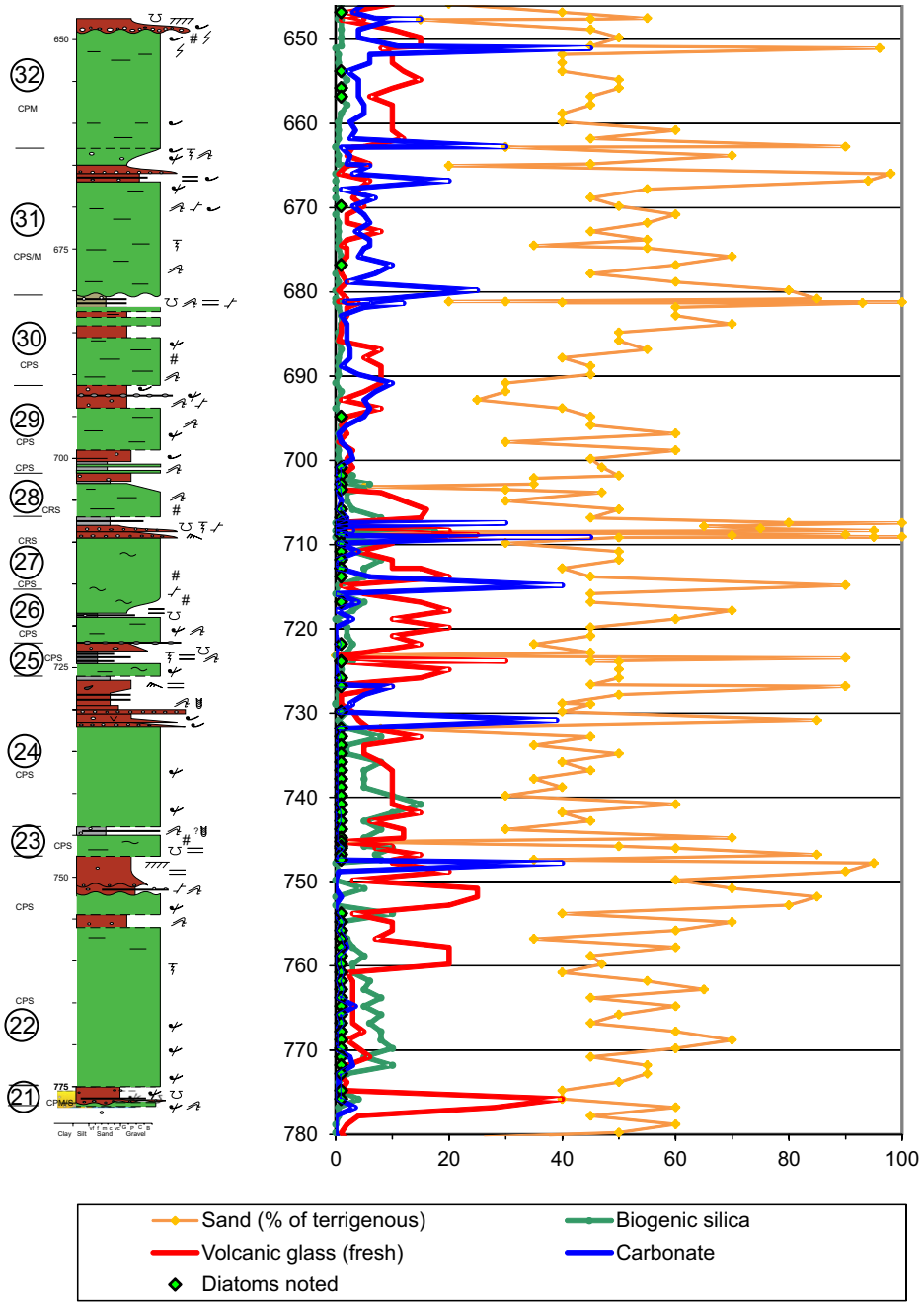

Figure 13. Composite Sequence 5 with smear slide data. See Figure 2 for a key to colors in the lithologic column and Figure 3B for graphics symbols. Abbreviations as in Figure 3 caption.

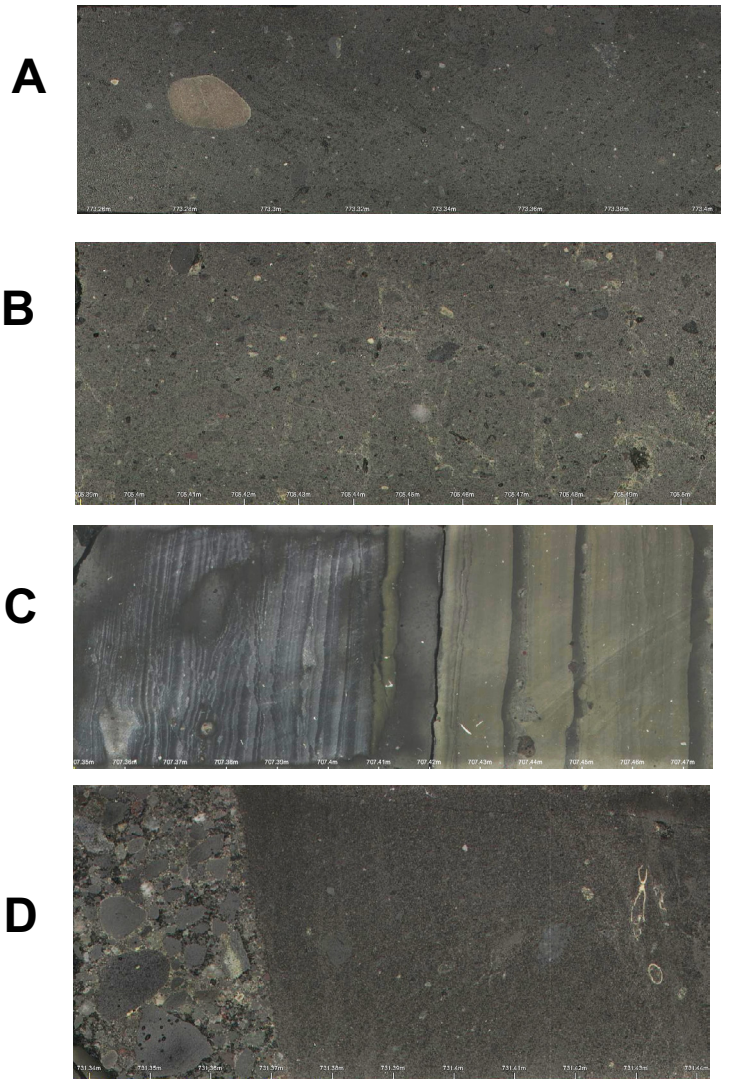

Figure 14. Composite Sequence 5 lithologies showing (A) clast-poor, sandy diamictite with rounded clast, (B) boxwork fractures, (C) conglomerate overlying shelly sandstone, (D) mm-bedded mudstone with dropstones.

span indicate a periodicity of around 40 k.y., consistent with the main control being obliquity. CS5 will be interpreted further in a later paper focused on the late early to middle Miocene interval of the core. In addition, Hauptvogel and Passchier (2012) describe the top part of CS5, above 650 m.

DISCUSSION

Variability of Ice Sheet Extent

The lithologies observed in intervals CS2 and CS4 indicate two periods of reduced ice influence in the early Miocene (Fig. 15). CS2 records the least ice-influenced interval of the early Miocene cored in AND-2A, spanning a time interval of around 50–60 k.y. CS4 records a prolonged ice-distal setting during deposition of the ~125-m-thick unit, with limited facies variation and an age span of about 700 k.y. The higher percentage of sandstone, mudstone and macrofossils suggests less glacially dominated conditions during CS4 times than during CS2 times, but there is sedimentological evidence supporting the presence of sea ice, ice shelf formation or icebergs, particularly in the upper part of CS4, with more open sea conditions at the top of CS4.

Variations in provenance indicate local, TAM glaciers reached the coast and were able to supply sediments during deposition of CS1 (Sandroni and Talarico, 2011; Iacoviello et al., 2015). The primarily ice-rafted sand in CS2 shows a large contribution from local metamorphic sources consistent with minor calving of local Transantarctic outlet glaciers (Iacoviello et al., 2015). CS3 and CS5 contain clasts and sand from farther south, perhaps with local TAM glaciers being landlocked and unable to supply iceberg-rafted debris. It is likely there was major ice advance and retreat during the period represented by the unconformity at the base of CS5, as this would account for the unconformity and the increase in volcanic glass (possibly due to unloading of both sediment and ice) in CS5. However, the basal sediments of CS5 are not clearly glacial lag moraines.

The overall picture for the early Miocene (spanning the period 20.2–17.35 Ma) is one of significant ice advance alternating with periods of ice retreat and hence likely changes in global climate, as recognized by Levy et al. (2016); such changes are now able to be modeled in a way consistent with known variations in oxygen isotopes and small variations in atmospheric concentrations of CO_2 (Gasson et al., 2016).

Paleoenvironments and Eustatic Sea Level Changes

Quantitative paleobathymetries and bottom current strengths in the Ross Sea during the early Miocene are difficult to assess, particularly as Ross Island and McMurdo Sound would not have been present as physiographic entities. Ross Sea Surface Water (RSSW) in the top 100 m in the Ross Sea has a slightly lower salinity due to ice-melt (Jacobs et al., 1970), so high sediment-load glacial discharges at that depth would more likely be underflow plumes. Deeper water settings would be more conducive to overflow plumes, above a basal, higher salinity water layer (e.g., High Salinity Shelf Water, HSSW, of Jacobs et al., 1970). The high salinity pore waters measured in AND-2A (Fielding et al., 2008; Frank et al., 2010) would be consistent with HSSW and therefore water depths significantly greater than 100 m for periods of early Miocene deposition, though the presence or absence of a seafloor sill seaward of the drill site that could restrict mixing would influence this effect. Eustatic sea-level

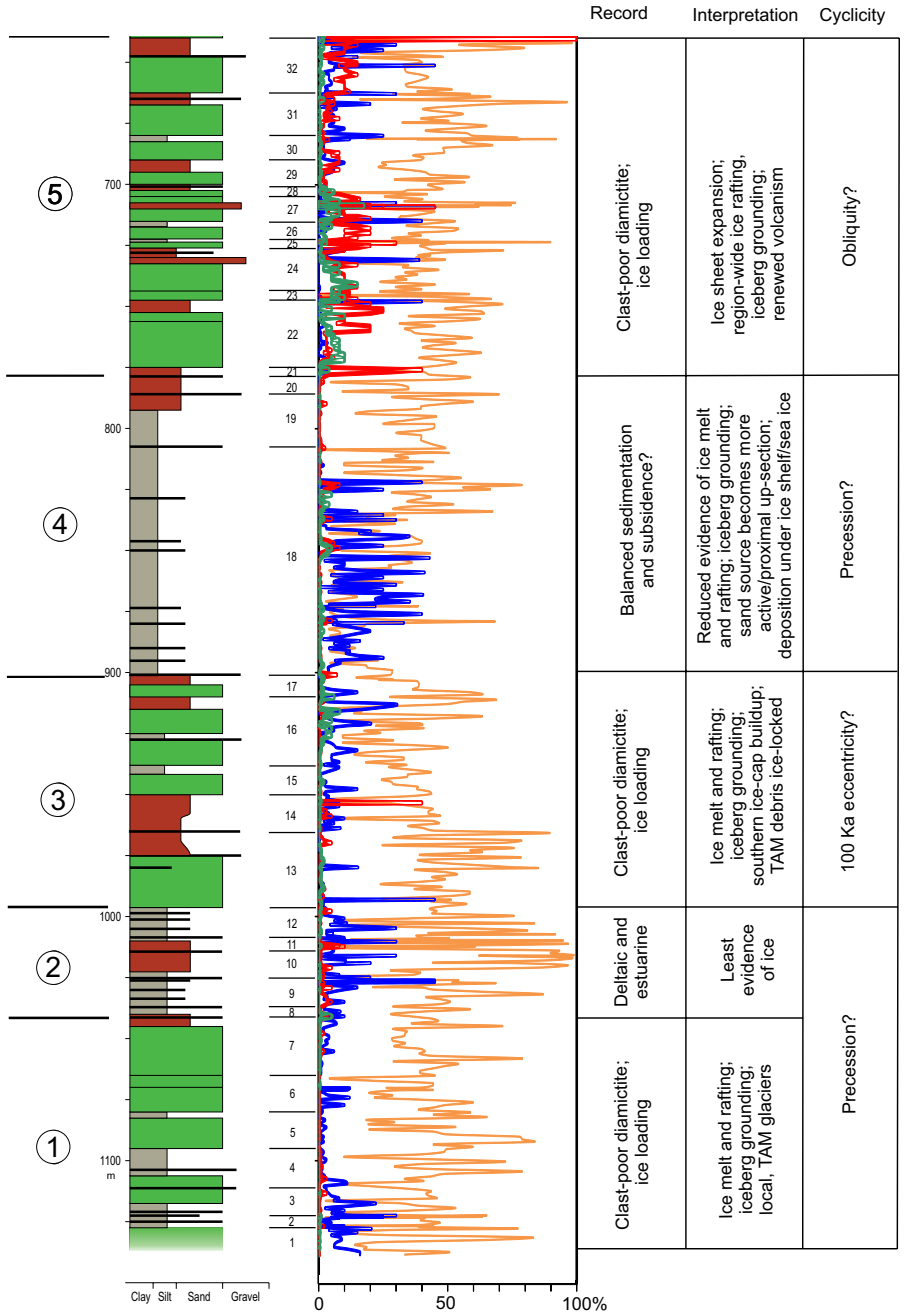

Figure 15. Summary of interpretations. See Figure 2 for color codes. TAM—Transantarctic Mountains.

changes of around 30 m were derived in simulations based on ANDRILL data by Gasson et al. (2016), though gravitational and isostatic rebound edge effects would need to be estimated to refine local relative sea-level changes at the drill site.

Such edge effects could include sea-level rises that post-date initial glacio-eustatic falls by about 1.7 m.y. (Stocchi et al., 2013), with any changes in relative sea level inferred for the oldest 1.7 m.y. of the interval cored by AND-2B being controlled by older events for which we have no proximal record. Thus sea level during deposition of CS4 could have been influenced by events older than the sediments drilled in AND-2B.

At depths shallower than 100 m, present Antarctic Surface Water flow is toward the west along the ice shelf front at 1.5 $m.s^{-1}$, driven by prevailing north and northwest winds blowing off the ice shelf (Jacobs et al., 1970). These current strengths are sufficient to move fine-grained sediment on the sea floor and such currents could account for some of the sharp tops in the mm-bedded units. Flow in basins >500 m deep is generally <0.1 $m.s^{-1}$ and varies in magnitude and direction (Jacobs et al., 1970). Currents often generate significant nepheloid layers in the bottom 50 m of the water column (Dinniman et al., 2003) and circulation of mud and diatom debris is likely to have occurred in early Miocene times. Jaeger et al. (1996) modeled current flows in the Ross Sea and concluded fine (biogenic) material from surface waters could be transported tens of kilometers before settling through ~500 m of water. This is deeper than inferred for early Miocene times at AND-2A, but this transport during settling suggests the presence of small volumes of fine-grained biogenic material in AND-2A might not be a good indicator of the presence or absence of an ice shelf. Fine sediment plumes could also be carried tens of kilometers laterally from source prior to deposition.

CS1 is interpreted as sub-polar, perhaps with slightly warmer conditions evident higher in the unit. The local provenance near the base of the unit suggests TAM glaciers extended to this part of the Ross Sea. The deltaic sediments inferred in CS2 were probably not deposited in large, shelf-break trough mouth fans as described by Vorren and Laberg (1997), as seismic lines near the drill site show no evidence for a shelf break or large, shelf troughs or incisions (Florindo et al., 2008). Seismic resolution at this level is not sufficiently good to resolve these three cycles or any downlap seismic architecture as would be expected from delta progradation. While CS2 records ice-free conditions at the drill site, the presence of some IRD indicates icebergs were present at times, and the appearance of coarse clasts of SM provenance at the top of CS2 suggests renewed glacial activity and ice-rafting started prior to CS3. CS3 records grounded ice at the drill site, but not with local, KB provenance. This could mean that icebergs from the south were occasionally grounded at the drill site, with local TAM glaciers land-locked and unable to supply debris to the site. CS4 is enigmatic, being thick, mudstone-dominated yet having fine IRD. There is no evidence for grounded ice at the drill site but sea ice is inferred for early CS4 time, ice shelf or stable sea ice for the upper portion of CS4, and perhaps more open marine conditions at the top. Provenance changes within CS4 indicate variations in ice cover occurred during deposition of the unit. CS5 comprises rafted debris from multiple sources, consistent with active, region-wide ice advance and retreat, with ice-loading from large bergs (or glaciers) at times.

Coincidence of both sedimentary dip data and pebble provenance determinations is sparse. However, there appears to be no consistent relationship between pebble clast provenance and paleocurrent directions, with packages containing southern (SM and CB) clasts having SE-, SW- and NE-dipping foresets. This would be consistent with transport of pebbles by icebergs (influenced by surface gyres or winds) or that pebble clasts that were deposited by traction currents were reworked by local paleocurrents after they had been rafted to the drill site region.

Cyclicity

Vertical sediment rainout is greatest during and after breakup of sea ice and this might explain some of the small-scale cyclicity seen in the core. Teitler et al. (2010) recorded IRD in Pleistocene core at ODP Site 1090 from the South Atlantic Ocean during both glacials and interglacials, with absence only during glacial terminations, suggesting that the presence of IRD in the relatively ice-distal intervals of CS2 and CS4 does not preclude their recording interglacial phases.

Periodicity in CS1 and CS2 is consistent with ~21 k.y. precession but in CS3 the frequency might be closer to 100 k.y. eccentricity, with a possible return to precession in CS4. CS5 cyclicity is consistent with obliquity. Combined with provenance data, we suggest local, TAM glacial activity under precessional control in CS1 and more southern ice-cap variations under 100 k.y. eccentricity (CS3) and obliquity (CS5) control (Fig. 15).

Seasonal variations in current strength might account for elements of the cyclicity seen in mm-bedded units, but we commonly cannot readily discriminate seasonal from tidal bedforms. Padman et al. (2003) modeled modern tidal currents in the Ross Sea ranging from 1 $m.s^{-1}$ at the shelf break to 0.1–0.2 $m.s^{-1}$ in the central continental shelf area and ~0.05 $m.s^{-1}$ under the ice shelf. This indicates, perhaps counter-intuitively, that tidal current strengths in the early Miocene might have been greater in regions distal to the ice front (and land). In the absence of an ice shelf, however, tidal currents might have been stronger in paralic settings, perhaps during deposition of CS2. In spring and winter, the flow strength of the modern Ross Sea gyre currents increases, although currents are still largely dominated by tides (Pillsbury and Jacobs, 1985; Jaeger et al., 1996). The bundles of ~2–14 laminae in CS2 are interpreted as diurnal, weekly and perhaps semi-lunar cycles, though annual cycles cannot be excluded.

Correlation with Glacial Records Elsewhere in Antarctica

The only other drill hole to penetrate an early Miocene succession in the eastern Ross Sea area was CRP-1, ~50 km to the north and "east" of AND-2A (Barrett, 1998). The CRP-1 intervals of 108–120 m and 141–146 m, are relatively free of diamictite, and likely coincide with C6N and C6a.n1n (Roberts et al.,

to th

1998, their figure 8; Florindo et al., 2005, their figure 7). The shallower interval in CRP-1 was described as a shallow-marine deposit (Unit 6.2 after Cape Roberts Science Team, 1998), and the deeper interval as suspended sediment settling on a shelf with minor ice rafting (Unit 7.1, Hannah et al., 1998). In more detail, 110.38–114.10 m in CPR-1 was interpreted as near-shore to offshore non-glacial delta/shelf, representing two cycles, and 141.10–147.69 m as delta front/sandy shelf below wave base to glacimarine, showing glacial retreat then advance (Powell et al., 1998, their table 2). However, while it is tempting to correlate these two finer intervals in CRP-1 with CS4 and CS2, the interval in CRP-1 lies within the diatom *T. praefraga* Zone whereas CS4 and CS2 lie below it, so that correlation is not valid.

The Prydz Bay record (Hannah, 2006) is not as well dated as the AND-2A record, but is consistent with ice advance and retreat phases in the early Miocene. Hannah inferred one main advance and retreat between 20.8 and 19 Ma. The retreat might correlate with CS2, or alternatively CS4. The advance inferred after 19 Ma in Prydz Bay might correlate with the unconformity at the base of CS5.

Correlation with Oxygen Isotope Data

The unconformity between CS4 and CS5 has an inferred age between 17.75 and 18.7 Ma and might result from an ice advance associated with Mi-1ab at ca. 18.4 Ma (following Pekar and DeConto, 2006). No clear evidence for ice loading (e.g., boxwork fractures) was recognized in CS4 but any evidence of ice grounding at the drill site after deposition of CS4 could have been removed by erosion at the unconformity at the top of CS4.

The oxygen isotope record from Site 1090 (Billups et al., 2002; Pekar and DeConto, 2006) shows two negative excursions (relatively warmer periods or a reduction in ice volume) within the inferred age range of CS4 and, similarly, a cooling followed by a warm spike, in CS3. CS2 appears to be the same age as a pronounced, broad, negative excursion, although the AND-2A age model near the base of the core is not robust. CS1 was deposited around the time of the cool event inferred at isotope event Mi1aa at Site 1090 (Pekar and DeConto, 2006).

Stable oxygen isotope data from the Kerguelen Plateau (ODP Southern Ocean Site 747) indicate overall warming during the period of deposition of CS1 to CS3, punctuated by ~3 episodes of cooling, with substantial cooling around the time of deposition of CS5 (Billups et al., 2002). Detailed correlations are difficult to justify, given the present uncertainties of 100 k.y. or more in ages of the AND-2A succession. However, the correlation of CS5 with cooling associated with isotope event Mi1b (Fielding et al., 2011) seems strong.

CONCLUSIONS

This paper presents detailed sedimentological data for an ice-proximal early Miocene record from Antarctica for which there are few other comparable stratigraphic proxy records. Five Composite Sequences (CS1 to CS5) are recognized over the lower portion of the AND-2A cored interval with an inferred 17.35–20.2 Ma age. Using the adopted age model, we demonstrate contrasting periods of ice advance and retreat, data that is pivotal in refining climate models for the Antarctic region during the early Miocene. Our work concludes:

- The dominance of clast-poor diamictite and local presence of evidence for ice-loading in CS1, CS3 and CS5 indicates release of ice-bound debris transported by icebergs that were grounded occasionally at the drill site.
- CS2 records the least ice-influenced interval of the entire early Miocene core.
- CS4 is a >100-m-thick unit, indicating stable conditions with good preservation of the sedimentary record due to balanced sedimentation and subsidence rates.
- CS5 rests on an unconformity caused by the advance of southern glaciers associated with ice cap expansion; the erosion was substantial enough to trigger renewed volcanism in the Mount Morning area.
- Local, TAM glacial activity occurred under precessional control in CS1, with more southerly ice-cap buildup under perhaps 100 k.y. eccentricity, and obliquity control during CS 3 and CS5 respectively.
- The overall picture for the early Miocene is one of significant ice advance and retreat, and we conclude that Antarctic ice sheets varied significantly in extent during the early Miocene, with grounded ice at times reaching farther than the current extent and at times retreating substantially to prolonged ice-free conditions at the drill site. Global climate models for the early Miocene (prior to the early Miocene start of the middle Miocene warm period) should be compatible with such large-scale ice sheet fluctuations.

ACKNOWLEDGMENTS

We thank Steve Petrushak for preparation of thin sections, and Josh Reed for assistance with PSICAT data and Corelyzer images and the curators who handled the core. We particularly thank the drillers for great core recovery and quality of the core. We thank I.M. Browne (University of South Florida), and journal referees Eugene Domack and an anonymous reviewer for their helpful comments. The ANDRILL Program is a multinational collaboration between the Antarctic Programs of Germany, Italy, New Zealand and the United States. Antarctica New Zealand is the project operator, and has developed the drilling system in collaboration with Alex Pyne at Victoria University of Wellington and Webster Drilling and Enterprises Ltd. Scientific studies are funded by the U.S. National Science Foundation, New Zealand Foundation for Research Science and Technology (via GNS Science), Royal Society of New Zealand Marsden Fund, the Italian Antarctic Research Programme (PNRA), the German Research Foundation (DFG) and the Alfred Wegener Institute for Polar and Marine Research (Helmholtz Association of German Research Centres). Antarctica New Zealand supported the drilling team at Scott Base; Raytheon Polar Services supported the science team at McMurdo Station and the Crary Science and Engineering Laboratory. The ANDRILL Science Management Office at the University of Nebraska–Lincoln, USA, provided science planning and operational support.

REFERENCES CITED

Acton, G., Crampton, J., Di Vincenzo, G., Fielding, C., Florindo, F., Hannah, M.J., Harwood, D.M., Ishman, S.E., Johnson, K., Jovane, L., Levy, R., Lum, H.B., Marcano, M.C., Mukasa, S.B., Ohneiser, C., Olney, M., Riesselman, C., Sagnotti, L., Stefano, C., Strada, E., Taviani, M., Tuzzi, E., Verosub, K.L., Wilson, G.S., and Zattin, M., 2008, Preliminary Integrated chronostratigraphy of the AND-2A core, ANDRILL Southern McMurdo Sound Project Antarctica, *in* Harwood, D.M., Florindo, F., Talarico, F., and Levy, R.H., eds., Studies from the ANDRILL, Southern McMurdo Sound Project, Antarctica: Terra Antartica, v. 15, p. 211–220.

Bann, K.L., and Fielding, C.R., 2004, An integrated ichnological and sedimentological comparison on non-deltaic shoreface and subaqueous delta deposits in Permian reservoir units of Australia, *in* McElroy, D., ed., The Application of Ichnology to Paleoenvironmental and Stratigraphic Analysis: Lyell Meeting 2003: Geological Society of London Special Publication 228, p. 273–310, https://doi.org/10.1144/GSL.SP.2004.228.01.13.

Barrett, P.J., 1998, Studies from the Cape Roberts Project, Ross Sea, Antarctica: Scientific Report of CRP-1, Overview: Terra Antartica, v. 5, p. 255–258.

Billups, K., Channell, J.E.T., Zachos, J., 2002, Late Oligocene to early Miocene geochronology and paleoceanography from the subantarctic South Atlantic: Paleoceanography and Paleoclimatology, v. 17, p. 4-1–4-11, https://doi.org/10.1029/2000PA000568.

Cape Roberts Science Team, 1998, Initial Report on CRP-1, Cape Roberts Project, Antarctica: Terra Antartica, v. 5, p. 187.

Chewings, J.M., Atkins, G.B., Dunbar, G.B., Golledge, N.R., and Alloway, B.V., 2011, Aeolian 'dust' flux in McMurdo Sound, SW Ross Sea, Antarctica, *in* Litchfield, N.J., and Clark, K., eds., Abstract volume, Geosciences Conference, Nelson, 27 November–1 December: Geoscience Society of New Zealand Miscellaneous Publication v. 130A, p. 23 (poster).

Cowan, E.A., and Powell, R.D., 1990, Suspended sediment transport and deposition of cyclically interlaminated sediment in a temperate glacial fjord, Alaska, USA, *in* Dowdeswell, J.A., and Scourse, J.D., eds., Glacimarine Environments: Processes and Sediments: Geological Society of London Special Publication 53, p. 75–89, https://doi.org/10.1144%2FGSL.SP.1990.053.01.04.

Cowan, E.A., Cai, J., Powell, R.D., Clark, J.D., and Pitcher, J.N., 1997, Temperate glacimarine varves: An example from Disenchantment Bay, Southern Alaska: Journal of Sedimentary Research, v. 67, p. 536–549.

Cowan, E.A., Cai, J., Powell, R.D., Seramur, K.C., and Spurgeon, V.L., 1998, Modern tidal rhythmites deposited in a deep-water estuary: Geo-Marine Letters, v. 18, p. 40–48, https://doi.org/10.1007/s003670050050.

Di Roberto, A., Del Carlo, P., Rocchi, S., and Panter, K.S., 2012, Early Miocene volcanic activity and paleoenvironment conditions recorded in tephra layers of the AND-2 core (southern McMurdo Sound, Antarctica): Geosphere, v. 8, p. 1342–1355, https://doi.org/10.1130/GES00754.1.

Di Vincenzo, G., Bracciali, L., Del Carlo, P., Panter, K., and Rocchi, S., 2010, ^{40}Ar-^{39}Ar dating of volcanogenic products from the AND-2A core (ANDRILL Southern McMurdo Sound Project, Antarctica): Correlations with the Erebus Volcanic Province and implications for the age model of the core: Bulletin of Volcanology, v. 72, p. 487–505, https://doi.org/10.1007/s00445-009-0337-z.

Dinniman, M.S., Klinck, J.M., and Smith, W.O., Jr., 2003, Cross-shelf exchange in a model of Ross Sea circulation and biogeochemistry: Deep-Sea Research Part II: Topical Studies in Oceanography, v. 50, p. 3103–3120, https://doi.org/10.1016/j.dsr2.2003.07.011.

Dowdeswell, J.A., Elverhøi, A., and Spielhagen, R., 1998, Glacimarine sedimentary processes and facies on the polar North Atlantic margins: Quaternary Science Reviews, v. 17, p. 243–272, https://doi.org/10.1016/S0277-3791(97)00071-1.

Elverhøi, A., 1984, Glacigenic and associated marine sediments in the Weddell Sea, fjords of Spitsbergen and the Barents Sea: A review: Marine Geology, v. 57, p. 53–88, https://doi.org/10.1016/0025-3227(84)90195-6.

Fenies, H., De Resseguier, A., and Tastet, J.-P., 1999, Intertidal clay-drape couplets (Gironde estuary, France): Sedimentology, v. 46, p. 1–15, https://doi.org/10.1046/j.1365-3091.1999.00196.x.

Field, B.D., and Atkins, C., 2012, Characterization of fine grained sediment in the AND-2A drillhole core using QEMscan: GNS Open-File Science Report 2012/42, 8 p.

Fielding, C.R., Atkins, C.B., Bassett, K.N., Browne, G.H., Dunbar, G.B., Field, B.D., Frank, T.D., Krissek, L.A., Panter, K.S., Passchier, S., Pekar, S.F., Sandroni, S., Talarico, F., and ANDRILL-SMS Science Team, 2008, Sedimentology and stratigraphy of the AND-2A core, ANDRILL Southern McMurdo Sound Project, Antarctica, *in* Harwood, D.M., Florindo, F., Talarico, F., and Levy, R.H., eds., Studies from the ANDRILL, Southern McMurdo Sound Project, Antarctica: Terra Antartica v. 15, p. 77–112.

Fielding, C.R., Browne, G.H., Field, B.D., Florindo, F., Harwood, D.M., Krissek, L.A., Levy, R., Panter, K.S., Passchier, S., and Pekar, S.F., 2011, Sequence stratigraphy of the ANDRILL AND-2A drillcore, Antarctica: A long-term, ice-proximal record of Early to Mid-Miocene climate, sea-level and glacial dynamism: Palaeogeography, Palaeoclimatology, Palaeoecology, v. 305, p. 337–351, https://doi.org/10.1016/j.palaeo.2011.03.026.

Florindo, F., Wilson, G.S., Roberts, A.P., Sagnotti, L., and Verosub, K.L., 2005, Magnetostratigraphic chronology of a Late Eocene to Early Miocene glacimarine succession from the Victoria Land Basin, Ross Sea, Antarctica: Global and Planetary Change, v. 45, p. 207–236, https://doi.org/10.1016/j.gloplacha.2004.09.009.

Florindo, F., Harwood, D.M., Talarico, F., Levy, R.H., and the ANDRILL-SMS Science Team, 2008, Background to the Southern McMurdo Sound Project: Terra Antartica, v. 15, p. 13–20.

Frank, T.D., Gui, Z, and the ANDRILL SMS Science Team, 2010, Cryogenic origin for brine in the subsurface of southern McMurdo Sound, Antarctica: Geology, v. 38, p. 587–590, https://doi.org/10.1130/G30849.1.

Franke, D., and Ehrmann, W., 2010, Neogene clay mineral assemblages in the AND-2A drill core (McMurdo Sound, Antarctica) and their implications for environmental change: Palaeogeography, Palaeoclimatology, Palaeoecology, v. 286, p. 55–65, https://doi.org/10.1016/j.palaeo.2009.12.003.

Gasson, E., DeConto, R.M., Pollard, D., and Levy, R.H., 2016, Dynamic Antarctic ice sheet during the early to mid-Miocene: Proceedings of the National Academy of Sciences of the United States of America, v. 113, p. 3459–3464, https://doi.org/10.1073/pnas.1516130113.

Gradstein, F.M., Ogg, J.G., and Smith, A.G., 2004, A geologic time scale: Cambridge University Press, Cambridge, United Kingdom, 610 p.

Hannah, M.J., 2006, The palynology of ODP site 1165, Prydz Bay, East Antarctica: A record of Miocene glacial advance and retreat: Palaeogeography, Palaeoclimatology, Palaeoecology, v. 231, p. 120–133, https://doi.org/10.1016/j.palaeo.2005.07.029.

Hannah, M.J., Wrenn, J.H., and Wilson, G.J., 1998, Early Miocene and Quaternary marine palynomorphs from Cape Roberts Project CRP-1, McMurdo Sound, Antarctica: Terra Antartica, v. 5, p. 527–538.

Harwood, D.M., Florindo, F., Talarico, F., and Levy, R., eds., 2008, Studies from the ANDRILL Southern McMurdo Sound Project, Antarctica: Terra Antartica, v. 15, 235 p.

Hauptvogel, D.W., and Passchier, S., 2012, Early–Middle Miocene (17–14 Ma) Antarctic ice dynamics reconstructed from the heavy mineral provenance in the AND-2A drill core, Ross Sea, Antarctica: Global and Planetary Change, v. 82–83, p. 38–50, https://doi.org/10.1016/j.gloplacha.2011.11.003.

Henrys, S.A., Wilson, T.J., Whittaker, J.M., Fielding, C.R., Hall, J.M., and Naish, T., 2007, Tectonic history of mid-Miocene to present, southern Victoria Land Basin, inferred from seismic stratigraphy, in McMurdo Sound, Antarctica, *in* Cooper, A.K., Raymond, C.R., et al., eds., Antarctica: A keystone in a changing world—Online Proceedings of the 10th ISAES: U.S. Geological Survey Open-File Report 2007-1047, Short Research Paper 049.

Hunze, S., Schröder, H., Kuhn, G., and Wonik, T., 2013, Lithostratigraphy determined from downhole logs in the AND-2A borehole, southern Victoria Land Basin, McMurdo Sound, Antarctica: Geosphere, v. 9, p. 63–73, https://doi.org/10.1130/GES00774.1.

Iacoviello, F., Giorgetti, G., Turbanti Memmi, I., and Passchier, S., 2015, Early Miocene Antarctic glacial history: New insights from heavy mineral analysis from ANDRILL AND-2A drill core sediments: International Journal of Earth Sciences, v. 104, p. 853–872, https://doi.org/10.1007/s00531-014-1117-3.

Jacobs, S.S., Amos, A.F., and Bruchhausen, P.M., 1970, Ross Sea oceanography and Antarctic bottom water formation: Deep-Sea Research, v. 17, p. 935–962.

Jaeger, J.M., Nittrouer, C.A., DeMaster, D.J., Kelchner, C., and Dunbar, R.B., 1996, Lateral transport of settling particles in the Ross Sea and implications for the fate of biogenic material: Journal of Geophysical Research, v. 101, p. 18479–18488, https://doi.org/10.1029/96JC01692.

Kominz, M., Browning, J.V., Miller, K.G., Sugarman, P.J., Misintseva, S., and Scotese, C.R., 2008, Late Cretaceous to Miocene sea-level estimates from the New Jersey and Delaware coastal plain coreholes: An error analysis: Basin Research, v. 20, p. 211–226, https://doi.org/10.1111/j.1365-2117.2008.00354.x.

Lear, C.H., Rosenthal, Y., Coxall, H.K., and Wilson, P.A., 2004, Late Eocene to early Miocene ice sheet dynamics and the global carbon cycle: Paleoceanography and Paleoclimatology, v. 19, PA4015, https://doi.org/10.1029/2004PA001039.

Lemmen, D.S., 1990, Glaciomarine sedimentation in Disraeli Fiord, high arctic Canada: Marine Geology, v. 94, p. 9–22, https://doi.org/10.1016/0025-3227(90)90100-X.

Levy, R.H., Harwood, D., Florindo, F., Sangiorgi, F., Tripati, R., von Eynatten, H., Gasson, E., Kuhn, G., Tripati, A., DeConto, R., Fielding, C., Field, B.D., Golledge, N.R., McKay, R., Naish, T.R., Olney, M., Pollard, D., Schouten, S., Talarico, F., Warny, S., Willmott, V., Acton, G., Panter, K., Paulsen, T., and Taviani, M., SMS Science Team, 2016, Antarctic ice sheet sensitivity to atmospheric CO_2 variations in the early to mid-Miocene: Proceedings of the National Academy of Sciences of the United States of America, v. 113, p. 3453–3458, https://doi.org/10.1073/pnas.1516030113.

Martin, A.P., Cooper, A.F., and Dunlap, W.J., 2010, Geochronology of Mount Morning, Antarctica: Two-phase evolution of a long-lived trachyte-basinite-phonolite eruptive center: Bulletin of Volcanology, v. 72, p. 357–371, https://doi.org/10.1007/s00445-009-0319-1.

McKay, R., Browne, G., Carter, L., Cowan, E., Dunbar, G., Krissek, L., Naish, T., Powell, R., Reed, J., Talarico, F., and Wilch, T., 2009, The stratigraphic signature of the late Cenozoic Antarctic ice sheets in the Ross Embayment: Geological Society of America Bulletin, v. 121, p. 1537–1561, https://doi.org/10.1130/B26540.1.

Mutti, E., and Sonnino, M., 1981, Compensation cycles: A diagnostic feature of turbidite sandstone lobes. International Association of Sedimentologists, 2nd European Meeting, Bologna, Italy, p. 120–123.

Naish, T., et al., 2009, Obliquity-paced Pliocene West Antarctic ice sheet oscillations: Nature, v. 458, p. 322–328, https://doi.org/10.1038/nature07867.

Naish, T.R., Levy, R.H., Powell, R.D., and MIS Science and Operations Team Members, 2006, Scientific Logistics Implementation Plan for the ANDRILL McMurdo Ice Shelf Project: ANDRILL Science Management Office, Lincoln, Nebraska, USA, Contribution 7, 138 p.

Nyland, R.E., Panter, K.S., Rocchi, S., Di Vincenzo, G., Del Carlo, P., Tiepolo, M., Field, B., and Gorsevski, P., 2013, Volcanic activity and its link to glaciation cycles: Single-grain age and geochemistry of Early to Middle Miocene volcanic glass from ANDRILL AND-2A core, Antarctica: Journal of Volcanology and Geothermal Research, v. 250, p. 106–128, https://doi.org/10.1016/j.jvolgeores.2012.11.008.

Ó Cofaigh, C., and Dowdeswell, J.A., 2001, Laminated sediments in glacimarine environments: Diagnostic criteria for their interpretation: Quaternary Science Reviews, v. 20, p. 1411–1436, https://doi.org/10.1016/S0277-3791(00)00177-3.

Padman, L., Erofeeva, S., and Joughin, I., 2003, Tides of the Ross Sea and Ross Ice Shelf cavity: Antarctic Science, v. 15, p. 31–40, https://doi.org/10.1017/S0954102003001032.

Panter, K.S., Talarico, F.M., Bassett, K., Del Carlo, P., Field, B., Frank, T., Hoffmann, S., Kuhn, G., Reichelt, L., Sandroni, S., Taviani, M., Bracciali, L., Cornamusini, G., von Eynatten, H., Rocchi, S., and the ANDRILL-SMS Science Team, 2008, Petrologic and geochemical composition of the AND-2A core, ANDRILL Southern McMurdo Sound Project, Antarctica: Terra Antartica, v. 15, p. 147–192.

Passchier, S., Browne, G., Field, B., Fielding, C.R., Krissek, L.A., Panter, K., Pekar, S.F., and ANDRILL-SMS Science Team, 2011, Early and Middle Miocene Antarctic glacial history from the sedimentary facies distribution in the AND-2A drill hole, Ross Sea, Antarctica: Geological Society of America Bulletin, v. 123, p. 2352–2365, https://doi.org/10.1130/B30334.1.

Passchier, S., Falk, C.J., and Florindo, F., 2013, Orbitally paced shifts in the particle size of Antarctic continental shelf sediments in response to ice dynamics during the Miocene climatic optimum: Geosphere, v. 9, p. 54–62, https://doi.org/10.1130/GES00840.1.

Pekar, S., and DeConto, R.M., 2006, High-resolution ice-volume estimates for the early Miocene: Evidence for a dynamic ice sheet in Antarctica: Palaeogeography, Palaeoclimatology, Palaeoecology, v. 231, p. 101–109, https://doi.org/10.1016/j.palaeo.2005.07.027.

Pfirman, S.L., and Solheim, A., 1989, Subglacial meltwater discharge in the open-marine tidewater glacier environment: Observations from Nordaustlandet, Svalbard Archipelago: Marine Geology, v. 86, p. 265–281, https://doi.org/10.1016/0025-3227(89)90089-3.

Pillsbury, R.D., and Jacobs, S.S., 1985, Preliminary observations from long-term current meter moorings near the Ross Ice Shelf, Antarctica, *in* Jacobs, S.S., ed., Oceanology of the Antarctic Continental Shelf: Washington, D.C., American Geophysical Union, Antarctic Research Series 43, p. 87–107, https://doi.org/10.1029/AR043p0087.

Pollard, D., and DeConto, R.M., 2009, Modeling West Antarctic ice sheet growth and collapse through the last five million years: Nature, v. 458, p. 329–332, https://doi.org/10.1038/nature07809.

Powell, R.D., Hambrey, M.J., and Krissek, L.A., 1998, Quaternary and Miocene glacial and climatic history of the Cape Roberts drillsite region, Antarctica: Terra Antartica, v. 5, p. 341–351.

Roberts, A.P., Wilson, G.S., Florindo, F., Sagnotti, L., Verosub, K.L., and Harwood, D.M., 1998, Magnetostratigraphy of Lower Miocene strata from the CRP-1 core, McMurdo Sound, Ross Sea, Antarctica: Terra Antartica, v. 5, p. 703–713.

Sandroni, S., and Talarico, F.M., 2011, The record of Miocene climatic events in AND-2A drill core (Antarctica): Insights from provenance analyses of basement clasts: Global and Planetary Change, v. 75, p. 31–46, https://doi.org/10.1016/j.gloplacha.2010.10.002.

Shackleton, N.J., and Kennett, J.P., 1975: Initial Reports of the Deep Sea Drilling Project, v. 29, p. 801–807.

Shevenell, A.E., and Kennett, J.P., 2007, Cenozoic Antarctic cryosphere evolution: Tales from deep-sea sedimentary records: Deep Sea Research Part II: Topical Studies in Oceanography, v. 54, p. 2308–2324, https://doi.org/10.1016/j.dsr2.2007.07.018.

Slatt, R.M., 2013, editor, Stratigraphic Reservoir Characterization for Petroleum Geologists, Geophysicists, and Engineers: Amsterdam, Netherlands, Elsevier B.V., Developments in Petroleum Science, v. 61, second ed., 671 p.

Smith, N.D., Phillips, A.C., and Powell, R.D., 1990, Tidal drawdown: A mechanism for producing cyclic sediment laminations in glaciomarine deltas: Geology, v. 18, p. 10–13, https://doi.org/10.1130/0091-7613(1990)018<0010:TDAMFP>2.3.CO;2.

SMS Science Team, 2010, An integrated age model for the AND-2A drill core, *in* Kontar, K., Harwood, D.M., Florindo, F., and Fischbein, S., compilers, ANDRILL Southern McMurdo Sound Project Science Integration Workshop, Erice, Italy, 6–11th April: ANDRILL Contribution, v. 16, p. 12–13.

Stocchi, P., Escutia, C., Houben, A.J.P., Vermeersen, B.L.A., Pijl, P.L., Brinkhuis, H., DeConto, R.M., Galeotti, S., Passchier, S., Pollard, D., and IODP Expedition 318 scientists, 2013, Relative sea level rise around East Antarctica during Oligocene glaciation: Nature Geoscience, v. 6, p. 380–384, https://doi.org/10.1038/ngeo1783.

Syvitski, J.P.M., 1989, On the deposition of sediment within glacier-influenced fjords: Oceanographic controls: Marine Geology, v. 85, p. 301–329, https://doi.org/10.1016/0025-3227(89)90158-8.

Talarico, F.M., and Sandroni, S., 2011, Early Miocene basement clasts in ANDRILL AND-2A core and their implications for paleoenvironmental changes in the McMurdo Sound region (western Ross Sea, Antarctica): Global and Planetary Change, v. 78, p. 23–35, https://doi.org/10.1016/j.gloplacha.2011.05.002.

Teitler, L., Detlef, A., Warnke, K.A., Venz, D.A., Hodell, S.B., Gersonde, R., and Teitler, W., 2010, Determination of Antarctic ice sheet stability over the last ~500 ka through a study of iceberg-rafted debris: Paleoceanography and Paleoclimatology, v. 25, p. PA1202, https://doi.org/10.1029/2008PA001691.

Visser, M.J., 1980, Neap-spring cycles reflected in Holocene subtidal large-scale bedform deposits: A preliminary note: Geology, v. 8, p. 543–546, https://doi.org/10.1130/0091-7613(1980)8<543:NCRIHS>2.0.CO;2.

Vorren, T.O., and Laberg, J.S., 1997, Trough mouth fans—Palaeoclimate and ice-sheet monitors: Quaternary Science Reviews, v. 16, p. 865–881, https://doi.org/10.1016/S0277-3791(97)00003-6.

Wang, D., and Hesse, R., 1996, Continental slope sedimentation adjacent to an ice-margin. II. Glaciomarine depositional facies on Labrador Slope and glacial cycles: Marine Geology, v. 135, p. 65–96, https://doi.org/10.1016/S0025-3227(96)00012-6.

Zachos, J., Pagani, M., Sloan, L., Thomas, E., and Billups, K., 2001, Trends, rhythms, and aberrations in global climate 65 Ma to present: Science, v. 292, p. 686–693, https://doi.org/10.1126/science.1059412.